Geological Magazine

www.cambridge.org/geo

Sea-level fluctuations in the late Middle Permian estimated from palaeosols of the Sichuan Basin, SW China

Jun Li[1,2], Zhong Han[3], Xingyue Wen[4], Gregory J. Retallack[5] and Chengmin Huang[1]

[1]Department of Environmental Science and Engineering, Sichuan University, Chengdu 610065, China; [2]College of Geography and Environmental Engineering, Lanzhou City University, Lanzhou 730070, China; [3]School of Earth Sciences and Engineering, Nanjing University, Nanjing, 210093, China; [4]School of Land and Resource, China West Normal University, Nanchong, 637002, China and [5]Department of Geological Sciences, University of Oregon, Eugene, Oregon, 97403, USA

Original Article

Cite this article: Li J, Han Z, Wen X, Retallack GJ, and Huang C (2020) Sea-level fluctuations in the late Middle Permian estimated from palaeosols of the Sichuan Basin, SW China. *Geological Magazine* **157**: 1333–1348. https://doi.org/10.1017/S0016756819001481

Received: 24 March 2019
Revised: 7 November 2019
Accepted: 3 December 2019
First published online: 15 January 2020

Keywords:
palaeopedology; palaeosols; carbonate microfacies; Emeishan basalt; Maokou Formation; limestone

Author for correspondence:
Chengmin Huang,
Email: huangcm@scu.edu.cn

Abstract

Two upper Middle Permian palaeosols, consisting of coal and pyrite intercalated with a 20 cm thick limestone, were found near Mount Emei in the SW Sichuan Basin, China. The macro- and micromorphology and physico-chemical properties, in conjunction with the mineralogical composition of the palaeosol horizons were investigated. This type of palaeosol is common within the Permian intertidal facies of the Upper Yangtze Craton. The section reflects fluctuations within the range of 0–25 m in relative sea-level, with the depositional environment changing from shallow-marine to littoral, followed by tidal-flat to littoral, and finally to continental volcanic rocks, based on a combination of palaeopedological and carbonate microfacies analyses. Such short-term relative sea-level fluctuations in late Middle Permian times in the SW Sichuan Basin of South China are consistent with the long-term falling trend on a global scale in late Middle Permian times, and may be related to regionally variable subsidence and global cooling. The combination of coastal palaeosol and carbonate microfacies analyses is proposed as an additional tool for estimating the amplitude of sea-level changes.

1. Introduction

The Middle Permian is characterized by several regression–transgression couplets, including a global large-scale regression during late Middle Permian times to the lowest level of the Phanerozoic Eon (Hallam & Wignall, 1999; Wardlaw *et al.* 2004; Haq & Schutter, 2008; Kofukuda *et al.* 2014). The regression–transgression events are stratigraphically recorded by Middle Permian marine deposits in South China, located in the palaeo-Tethyan region, including Guangxi (Qiu *et al.* 2014*a*), Guizhou (Shen & Xu, 2005) and Sichuan (Isozaki *et al.* 2008; Saitoh *et al.* 2013) provinces. Numerous studies have been conducted to investigate various aspects of the regression–transgression couplets coupled with relative sea-level variations in Middle Permian times (Chen *et al.* 1998; Wang & Sugiyama, 2000; Yang *et al.* 2004; Rygel *et al.* 2008; Bond & Wignall, 2009), e.g. sequence stratigraphy (Tong *et al.* 1999; Bhattacharya & Banerjee, 2015) and sedimentary facies analysis in conjunction with refined biostratigraphy (Isozaki *et al.* 2008; Wignall *et al.* 2009; Saitoh *et al.* 2013; Kofukuda *et al.* 2014; Qiu *et al.* 2014*a*). Additionally, a variety of proxies have been used to decipher the environmental and climatic responses to past sea-level fluctuations, including bulk rock and clay mineral compositions, total organic carbon (TOC) and Sr/Ca ratios (Adatte *et al.* 2002; Jarvis *et al.* 2008), stable isotopes (Stüben *et al.* 2002; Siddall *et al.* 2003; Olde *et al.* 2015), benthic and planktonic foraminifera and diatoms (Galeotti & Coccioni, 2002; Brett & Mclaughlin, 2009; Bak, 2015; Wendler *et al.* 2016), fossil coral reefs (Yamamoto *et al.* 2006; Camoin & Webster, 2015) and salt-marsh sediments (Shaw & Ceman, 1999; Brain *et al.* 2015), fossil plant and otolith assemblages (Sandoval *et al.* 2001; Girone, 2005; Jank *et al.* 2006; Beiranvand *et al.* 2013), carbonate microfacies (Han *et al.* 2016) and the organic molecular compound index method (Wang *et al.* 2015). Based on the palaeopedology of the Permian deposits, there have been extensive studies regarding palaeoclimate and palaeoenvironment reconstructions (Tabor & Montañez, 2005; Tabor *et al.* 2008, 2011); however, little attention has been paid to the palaeosols for the interpretation of sea-level changes.

Rygel *et al.* (2008) performed a meta-analysis on over 100 published Permian eustatic sea-level records that were based on a variety of proxies. While these authors attempted to normalize the results to account for the type of proxy that was used to reconstruct sea-level (e.g. Haq & Schutter, 2008; Bak, 2015; Olde *et al.* 2015), a number of challenges remain. The reason for this is that subtle changes in sedimentation may not be discernable from lithofacies

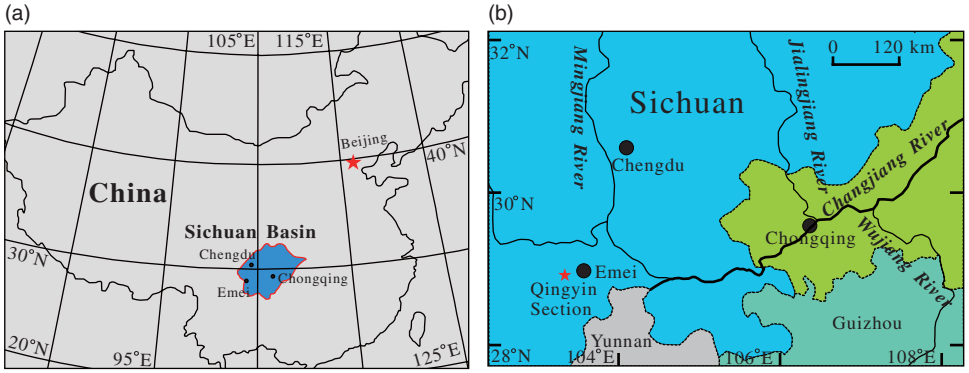

Fig. 1. (Colour online) Sketch map of the studied section in the southwestern Sichuan Basin, South China. (a) Location of the Sichuan Basin in China. (b) Location of the studied section in the Sichuan Basin.

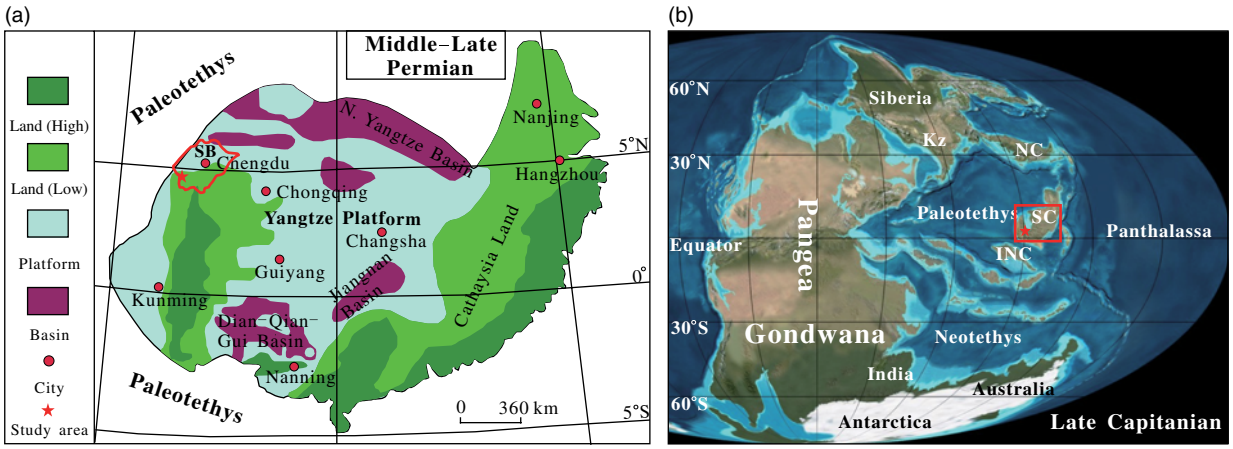

Fig. 2. (Colour online) Middle–Late Permian palaeogeography of (a) South China (modified from Wang & Jin, 2000; palaeolatitude after Zhang, 1997); SB – Sichuan Basin; and (b) the world (modified from Blakey, 2007); NC – North China; SC – South China; Kz – Kazakhstan.

or fossil communities related to changes in depositional depths away from coastal areas (Sames *et al.* 2016). Even though the pinning point method may quantitatively provide a relative sea-level history (Goldstein & Franseen, 1995), short-term sea-level variations may not be detected by sequence-stratigraphic data.

Palaeosols (fossil soils), unlike marine sedimentary records, are formed at the Earth's surface and provide a direct record of the environmental conditions at the time of their formation (Retallack, 2001; Sheldon & Tabor, 2009; Tabor & Myers, 2015). Even rare palaeosols can be useful for interpreting specific geological events (Gvirtzman *et al.* 1997; Álvaro *et al.* 2003; Narkiewicz & Retallack, 2014; Tsatskin *et al.* 2015), for example, acid-sulfate soils. Acid-sulfate soils, which form in coastal zones and mangrove swamp environments, alternating between exposure to air and inundation by the sea (Dent & Pons, 1995; Fanning *et al.* 2002; Fitzpatrick, 2003; Fitzpatrick *et al.* 2009; Ljung *et al.* 2009), are soils in which sulfuric acid may be produced, is being produced, or has been produced in certain amounts (Pons, 1973; Dent & Pons, 1995), and contain iron sulfide minerals (predominantly as the mineral pyrite (FeS_2)) or their oxidation products (e.g. jarosite, gypsum). Thus, acid-sulfate soils may be used to provide insights into relative sea-level fluctuations in response to environmental changes.

Palaeosols are common at the contact between the Middle Permian Maokou Formation and Emeishan basalts, which are distributed extensively in Yunnan, Guizhou and Sichuan provinces of SW China (He *et al.* 2003, 2010). The hiatus provides an excellent opportunity to examine the palaeoenvironments at the transition between the Maokou Formation and Emeishan basalts. In this study, we collected samples of pyrite-bearing palaeosols developed at the contact between the Maokou limestone and Emeishan basalts in the Sichuan Basin of SW China. Our aim is to (1) examine the potential of coastal palaeosols as indicators of relative sea-level variations and other palaeoenvironmental changes; (2) provide a description of the palaeosols and their Permian distribution in SW China; and (3) to reveal the potential causes for short-term sea-level fluctuations in late Middle Permian times in the SW Sichuan Basin of South China.

2. Geological setting

The Sichuan Basin is a rhomboid-shaped sedimentary basin located in SW China (Tan *et al.* 2011; Zhu *et al.* 2015) (Fig. 1a) and has a surface area of ~180×10^3 km^2 (Zhao *et al.* 2011; Zhu *et al.* 2015). During Middle–Late Permian times, the Sichuan Basin of the South China platform was situated in the southwest of the Yangtze plate (Fig. 2a), lying in the palaeo-equatorial eastern palaeo-Tethys (Wang & Jin, 2000) (Fig. 2b).

https://doi.org/10.1017/S0016756819001481 Published online by Cambridge University Press

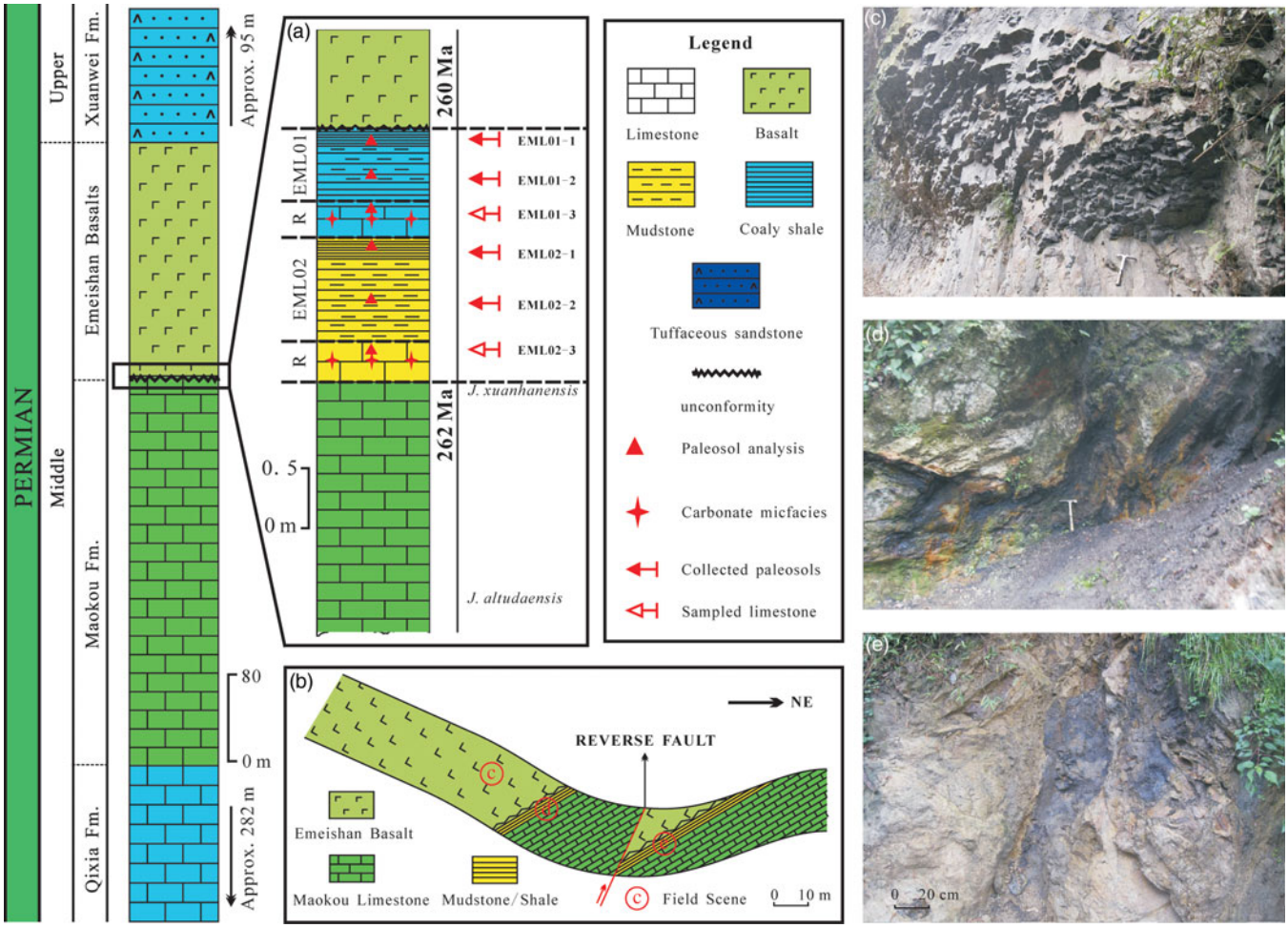

Fig. 3. (Colour online) (a) Stratigraphic framework of the Middle and Upper Permian in the SW Sichuan Basin; triangle – location of sampling sections. The conodont zones, which were dominated by *J. xuanhanensis* and *J. altudaensis*, are derived from Lai *et al.* (2008) and Sun *et al.* (2010). (b) Sketch map of the reverse fault. (c) Emeishan basalts unconformably overlying the Maokou Formation. (d) The hiatus between the Emeishan basalts and Maokou Formation. (e) The tree stump residues preserved in the Maokou Formation owing to the reverse fault. Hammer for scale is ~28 cm long.

In the Mount Emei region, the Maokou Formation conformably overlies the Middle Permian Qixia Formation, composed of ~280 m thick dark limestone, and is unconformably overlain by the Emeishan volcanic successions, which have a thickness of ~230 m (Bureau of Geology and Mineral Resources of Sichuan Province, 1991) (Fig. 3). The Maokou Formation consists mainly of ~345 m of medium-bedded to massive limestone and contains a Tethyan marine fauna of fusulinids, brachiopods, gastropods, rugose coral, calcareous algae and crinoids (He *et al.* 2003; Isozaki *et al.* 2004, 2008), as evidence of a shallow-marine carbonate-platform.

The studied section (29° 34′ 45.24″ N, 103° 24′ 39.92″ E) crops out near the Qingyin Power Station in the Mount Emei region of the SW Sichuan Basin (Fig. 1b). The section is ~2 m of mudstone and shale, with a 20 cm thick limestone, below the Emeishan basalts, and it sharply overlies the uppermost Maokou limestone, which contains remains of fish, ostracods and the conodonts *Jinogondolella xuanhanensis* and *Jinogondolella altudaensis* (Lai *et al.* 2008; Sun *et al.* 2010) (Fig. 3a). The 20 cm thick limestone between the mudstone and shale is dominated by *Hindeodus excavatus* (Lai *et al.* 2008).

The palaeosols are younger than the underlying Maokou limestone and older than the Emeishan basalts. The overlying Emeishan basalts are stratigraphically well constrained to the upper Middle Permian (260 Ma) (Huang *et al.* 2016), determined by zircon SHRIMP U–Pb measurements (Zhou *et al.* 2002; He *et al.* 2007; Zi *et al.* 2010), ID-TIMS results for the basalts (Shellnutt *et al.* 2012) and magnetostratigraphic and bio-lithostratigraphic observations (Jin & Shang, 2000; Ali *et al.* 2005). The conodont *J. xuanhanensis* from the limestone underlying the palaeosols in the section (Sun *et al.* 2010) points to a late Capitanian (~262 Ma) age for the Maokou limestone. Jin & Shang (2000) have also assigned the limestone below the Emeishan basalts to the upper Middle Permian based on conodonts and fusulinids. Thus, the palaeosols between the Maokou limestone and Emeishan basalts developed between ~262 and ~260 Ma, close to the Middle–Late Permian transition. Moreover, the palaeosol section at Qingyin was within the tropical zone (palaeolatitude ~5° N) in Middle Permian times (Zhang, 1997).

3. Sampling and laboratory analysis

Samples (EML01 and EML02) were taken from each horizon (Fig. 3a), air dried, sieved (<2 mm) and ground, then used to analyse the chemical properties of the palaeosol (e.g. carbonate content, TOC and sulfur), physical properties (e.g. colour), mineral

https://doi.org/10.1017/S0016756819001481 Published online by Cambridge University Press

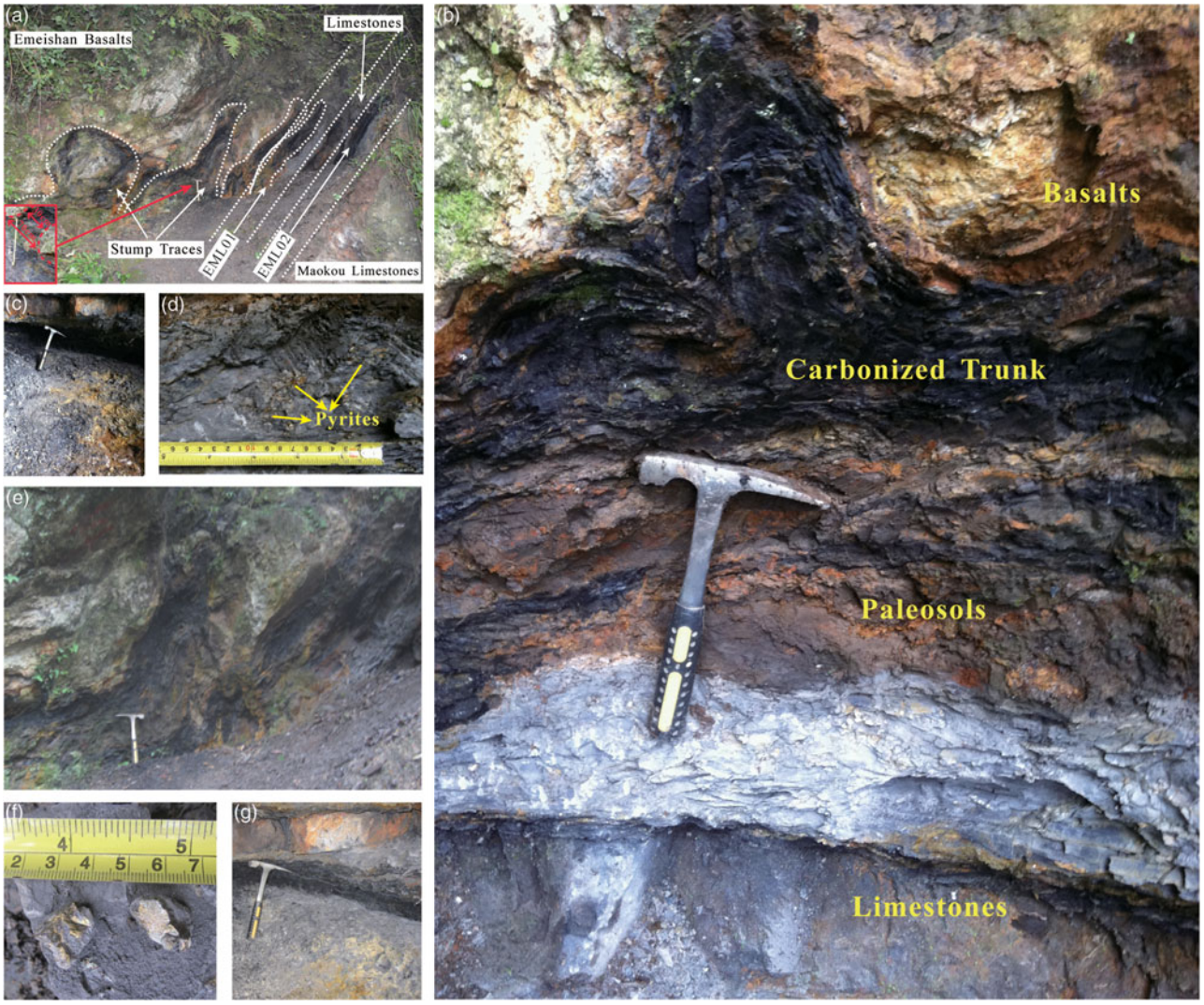

Fig. 4. (Colour online) Field photographs in the studied area. (a) Emeishan basalts unconformably overlying the Maokou Formation. (b) EML01 palaeosol. (c) EML02 palaeosol. (d) The pyrite-bearing Bg horizon in the EML02 palaeosol. (e) Close-up of tree stumps showing tree trunk fossil buried in the contact between the Emeishan basalts and Maokou Formation. (f) Pyrite crystals from the EML01 palaeosol. (g) Close-up of EML02 palaeosol. Hammer for scale is ~28 cm long.

composition of the bulk palaeosols and weight percentages of the major and minor elements. Moreover, six limestone samples (Fig. 3a) were collected from the limestone of profiles EML01 (EML01-3-1, -2, -3) and EML02 (EML02-3-1, -2, -3); thus, three samples per limestone interval (Fig. 3) were used for carbonate microfacies (MF) determinations. The carbonate content in the samples was measured by adding diluted 1 N HCl to produce CO_2, and then by converting the volume of CO_2 into carbonate concentration (%) (Dreimanis, 1962), and the organic carbon content was determined by the Walkley-Black titration method (Singer & Janitzky, 1987). The analysed error for the carbonate and organic carbon content was lower than 1 % and 0.5 %, respectively. Total sulfur (TS) content was determined using the barium sulfate turbidimetry spectrophotometry method (Fu *et al.* 2007) and has an error of ±0.005 %. Colour was identified following the Munsell soil colour system (Munsell Color, 2000).

The bulk mineralogy was detected using X-ray diffractometry (XRD) (Model X-Pert, produced by the Philips Company) with a voltage of 50 kV and a current of 35 mA at Sichuan University, China. Major and trace elements of the samples were analysed by X-ray fluorescence spectrometry (PW2403 X, Holland) at the Key Laboratory of West China's Environmental System, Lanzhou University, China. Analytical uncertainty was typically lower than 0.1 % for major elements, and 0.1–2 ppm for most trace elements. Thin-sections of individual palaeosols were prepared for micromorphological observation using a polarizing petrographic microscope to view and a camera to capture images, and were described using the micromorphological terminology of Bullock *et al.* (1985) and Stoops *et al.* (2010). Carbonate microfacies were described based on the nomenclature of Dunham (1962) and interpreted according to Flügel (2010).

4. Results

4.a. Palaeosol description and analysis

Two palaeosols (EML02 and EML01) were identified in a 2 m thick zone marking the contact between the Maokou Formation and Emeishan basalts in the SW Sichuan Basin based on several large tree stumps, abundant root traces and obvious soil structures and horizons (Fig. 4b, c, d, f). The older palaeosol was named EML02 and the younger one EML01 (Fig. 4a, b, c). These palaeosols can be interpreted using comparisons with the properties of modern soils.

https://doi.org/10.1017/S0016756819001481 Published online by Cambridge University Press

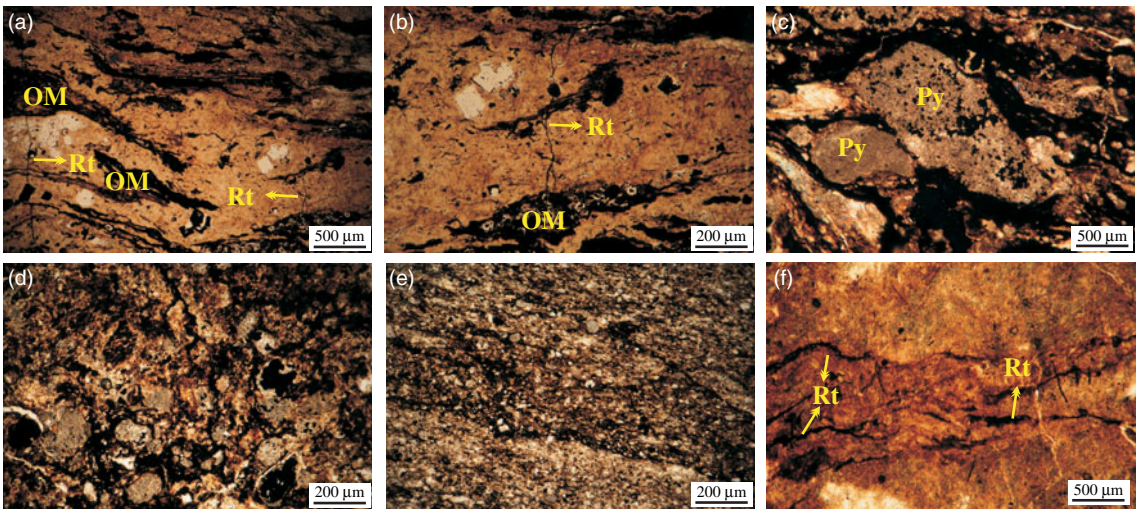

Fig. 5. (Colour online) Photomicrographs of pedogenic features observed in thin-sections of vertically oriented palaeosol samples. PPL – plane-polarized light. (a) Abundant organic material (OM), and fine and vertical downward-bracing roots (Rt; dark colour) in the EML01 palaeosol (Ah horizon, PPL). (b) Close-up view on the left side of image (a) showing fragments and fine and vertical downward-bracing roots (dark colour) in the EML01 palaeosol (Ah horizon, PPL). (c) Pyrite (Py) framboids and plant material (dark colour) in the EML01 palaeosol (Bg horizon, PPL). (d) Organic material infilling the interstices between limestone fragments in the EML01 palaeosol (Bg horizon, PPL). (e) Limestone fragments and organic material mixed in the EML01 palaeosol (Bg horizon, PPL). (f) Strongly ferruginized fossil plant material within the groundmass of the EML02 palaeosol (Bg horizon, PPL).

4.a.1. Macro- and microscopic description of the palaeosols

Both of the palaeosols (EML02 and EML01) are mudstone or shale, and have a clear and sharp upper and lower lithological boundary (Fig. 4). There is a 20 cm thick limestone bed (Sample No. EML01-3), which is greenish-grey in colour (5BG 6/1), between the two palaeosols (Figs 3a, 4a). The palaeosol EML02 overlies limestones of the Maokou Formation, and the palaeosol EML01 overlies the thin bed of limestone.

Palaeosol EML02 has an 18 cm thick black (N 2.5/1) organic-rich (Ah) horizon, which has converted to a coal seam that is grey in colour (N 25/1) owing to diagenesis. The 60 cm thick Bg horizon of palaeosol EML02 has yellowish brown (10YR5/6) mottles of iron-oxide-stained mudstone. Large amounts of pyrite are scattered through the Bg horizon (Fig. 4d). In thin-sections, root traces are generally horizontally to sub-horizontally oriented in the Bg horizon, suggesting a high water table (Fig. 5f). The transition between the Bg horizon and the underlying limestone is abrupt. This limestone of the Middle Permian Maokou Formation is bluish grey (5PB 6/1) in colour and contains abundant conodonts (*J. xuanhanensis*).

Overlain by the Emeishan basalts, the EML01 palaeosol consists of an Ah–Bg profile with a thickness of 55 cm. The organic horizon (Ah) has a thickness of 15 cm (Fig. 4b). Root traces are evident, reaching a depth of 50 cm, with a black colour (N 2.5/1). In particular, a carbonized tree trunk, which can be recognized by downward branching, was abruptly terminated by deposition of basalt lava and remained perpendicular in the Ah horizon (Fig. 4a, e). Some 70 cm of the trunk base width is preserved in a bedding plane exposure (Fig. 4a). In thin-section *in situ* carbonaceous roots are mostly horizontally branching, but a few fine rootlets with root hairs are vertically oriented and tapering downward in the Ah horizon (Fig. 5a, b). The Bg horizon has a thickness of 40 cm and shows colours varying from dark greyish brown (10YR 4/2) with prominent yellowish brown (10YR 5/8) iron-oxide mottles to bluish grey (5PB 6/1) with a massive blocky ped structure. Abundant pyrite crystals are found in the Bg horizon with variable diameters from 5 to 10 mm (Fig. 4f). The thin-section also exhibits similar pedogenic features in this horizon (Fig. 5c). Framboidal pyrite precipitation associated with organic material within the soil matrix is evident (Fig. 5c). In addition, mixed limestone fragments and organic material were distributed in the Bg horizon of palaeosol EML01 (Fig. 5d, e).

Throughout the section, significant differences in macromorphological properties, particularly regarding the tree root traces and *in situ* strata characteristics of the basalt–palaeosol–limestone sequences, are observed. More than three large tree stumps collapsed in the same direction (Figs 3d, e, 4a, e), and the strata experienced relative movement due to a small thrust fault (Fig. 3b, d, e). Regional tectonic movements that occurred in SW China during Middle Jurassic – Early Cretaceous times were largely responsible for the fault (Hou *et al.* 2002; Ali *et al.* 2004).

4.a.2. Chemical properties of the palaeosols

In the older (EML02) palaeosol, carbonate content in the surface horizon (4.6 %) is lower than in the Bg horizon (13.5 %), and carbonate in the Ah horizon of the younger (EML01) profile of 14.8 % is also lower than in the Bg horizon (29.1 %) (Fig. 6). Total organic carbon contents (TOC) in the EML02 samples fluctuate in the range of 0.9–2.3 %, whereas the EML01 palaeosol yielded TOC values of 1.8–2.6 % (Fig. 6). TS contents in the Ah and Bg horizons of the EML02 palaeosol are 0.13 % and 0.79 %, respectively. The Ah and Bg horizon of the EML01 palaeosol have TS contents of 0.21 % and 1.18 %, respectively (Fig. 6).

4.a.3. Elemental composition and geochemistry of the palaeosols

In the two analysed palaeosols, most of the major and trace elements show relatively higher contents in the Ah and Bg horizons compared to the underlying limestone, except for Ca and Mn (Fig. 7).

Obtained elements were used for calculating the molecular ratios, which have been used as a geochemical proxy for

https://doi.org/10.1017/S0016756819001481 Published online by Cambridge University Press

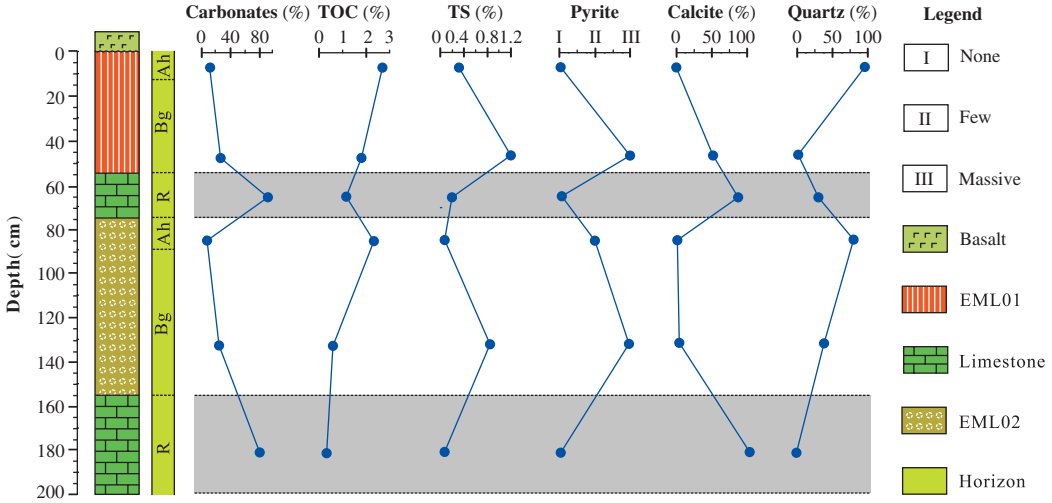

Fig. 6. (Colour online) Depth profiles of general characteristics and relative mineral content for the studied section.

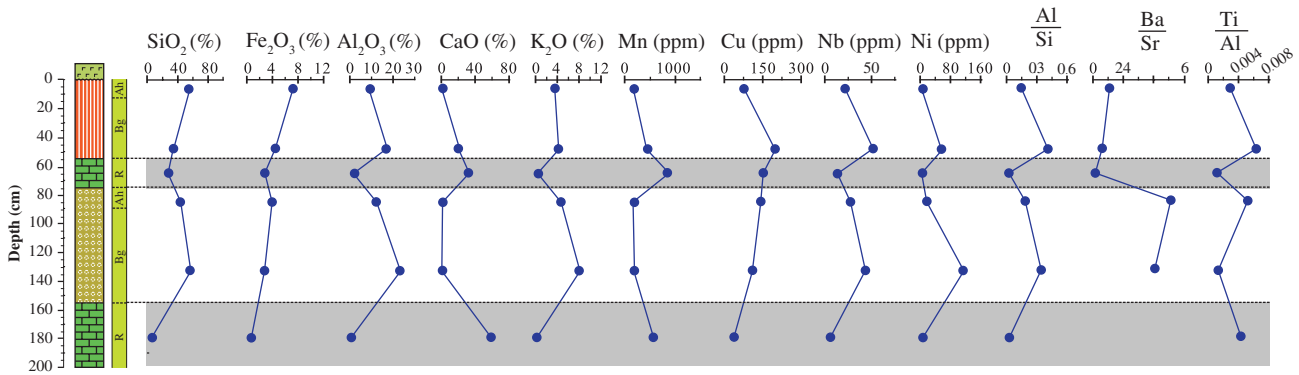

Fig. 7. (Colour online) Major- and trace-element contents varying with depth for the studied section.

evaluating pedogenic processes in palaeosols (Retallack, 2001; Sheldon & Tabor, 2009; Li *et al.* 2016), such as the index of clayeyness (Al/Si; Ruxton, 1968), provenance (Ti/Al; Retallack, 2001) and the barium/strontium ratio (Ba/Sr; Retallack, 2001). The Al/Si ratio is a function of the clayeyness of a palaeosol (Retallack, 2001), varying throughout the section from 0.03 to 0.44. Fe_2O_3 exhibits low concentrations (<10 %) in the two palaeosol profiles, generally decreasing slightly with depth, while the proportions of Al_2O_3, K_2O and Mn generally increase with depth in both palaeosols (Fig. 7). The Ti/Al ratio is used as a provenance indicator because Ti contents may be quite variable among different types of rocks, even as Al contents are relatively constant (Retallack, 2001; Sheldon & Tabor, 2009). Minor variation in Ti/Al values occurred in the examined horizons of the two palaeosols, ranging from 0.0016 to 0.0067 (Fig. 7). The Ba/Sr ratio is taken as a means of assessing weathering intensity (i.e. leaching) (Sheldon & Tabor, 2009), and the values measured in the profiles exhibit great variations, ranging from 0.08 to 5.10 (Fig. 7). The EML02 palaeosol shows high Ba/Sr values (>2). The SiO_2 content in the examined palaeosol profiles ranges from 33.9 % to 57.3 % (Fig. 7), which is high in comparison to the underlying limestone (generally between 4.8 % and 27.1 %). Moreover, the Al/Si ratio values in both palaeosols display an increasing trend from the Ah horizon to the Bg horizon suggesting clay formation, i.e. the development of a B horizon. In contrast, there is a decreasing trend in the Ba/Sr ratio from the surface to the subsurface Bg horizon of the examined palaeosol profiles (Fig. 7).

4.a.4. Mineral composition of the palaeosols

XRD analysis of EML02 shows that quartz is dominant, and illite and/or smectite and pyrite are present in small quantities in the Ah horizon (EML02-1) of the older (EML02) palaeosol. Pyrite, illite and/or smectite, gypsum, quartz and feldspar were identified in the Bg horizon (EML02-2) (Fig. 8). In addition, the Maokou limestone (EML02-3) was entirely composed of calcite.

The whole-rock X-ray patterns indicate that the Ah (EML01-1) horizon is mainly composed of quartz, whereas the Bg horizon (EML01-2) is dominated by calcite, pyrite and illite and/or smectite (Fig. 8). Micromorphological observations also confirm the presence of calcite and pyrite in the Bg horizon (Fig. 5c, e). The limestone sample (EML01-3) interbedded between the two palaeosols consists dominantly of calcite and quartz, with identified small amounts of aragonite. Moreover, large phenocrysts (EML01-2-1) are composed of pure pyrite (Fig. 8).

https://doi.org/10.1017/S0016756819001481 Published online by Cambridge University Press

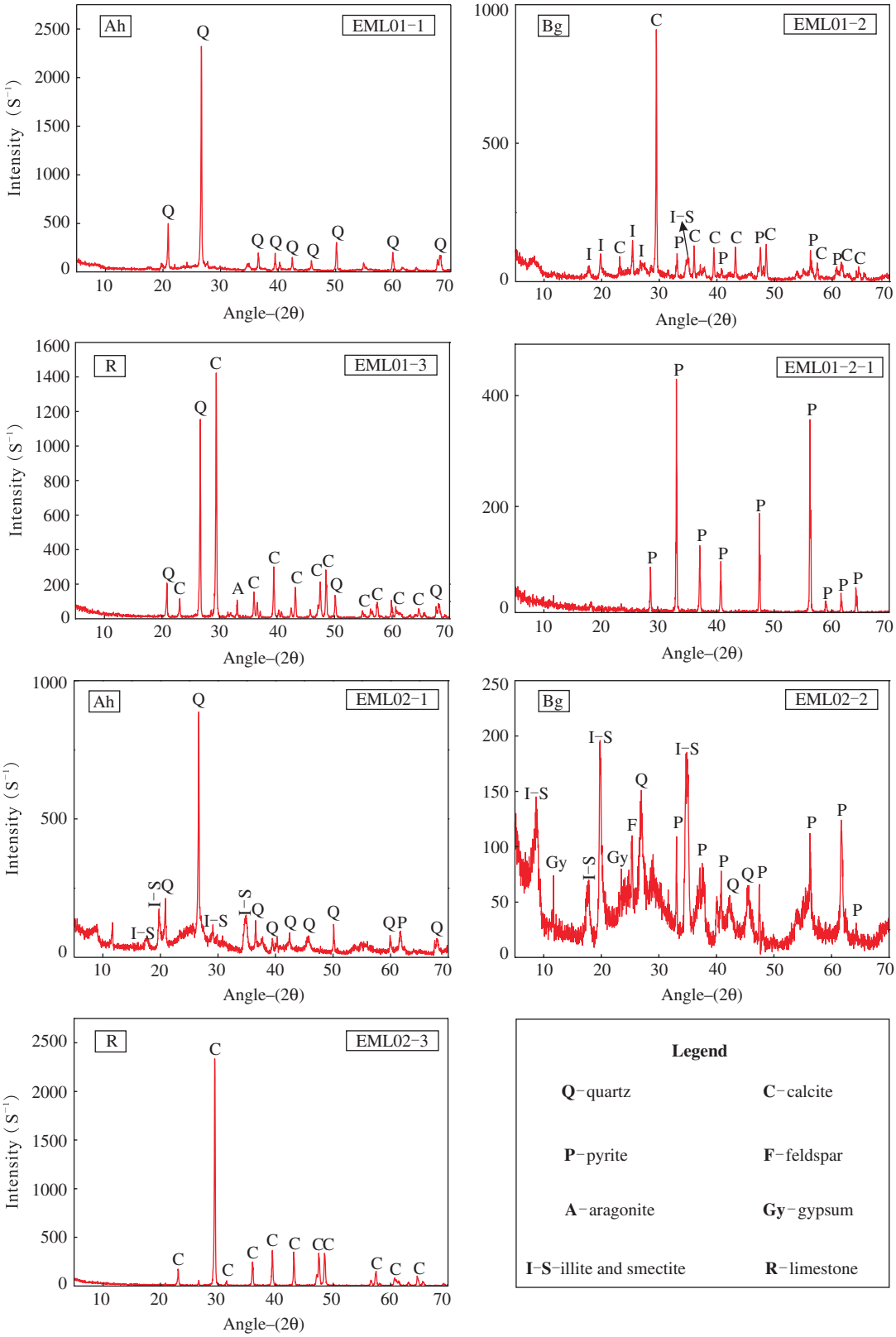

Fig. 8. (Colour online) Whole-rock X-ray patterns for the studied section.

4.b. Carbonate microfacies analysis

On the basis of texture, grain composition and fossil content, as well as the nomenclature of Dunham (1962), two characteristic microfacies were identified: bioclastic packstone (Fig. 9a) and ostracod mudstone/wackestone (Fig. 9b). These represent the bluish grey (5PB 6/1) limestone (EML02-3) (Fig. 3) at the base of palaeosol EML02, and the 20 cm thick greenish-grey (5BG 6/1) limestone (EML01-3) (Fig. 3) underlying the palaeosol EML01, respectively.

https://doi.org/10.1017/S0016756819001481 Published online by Cambridge University Press

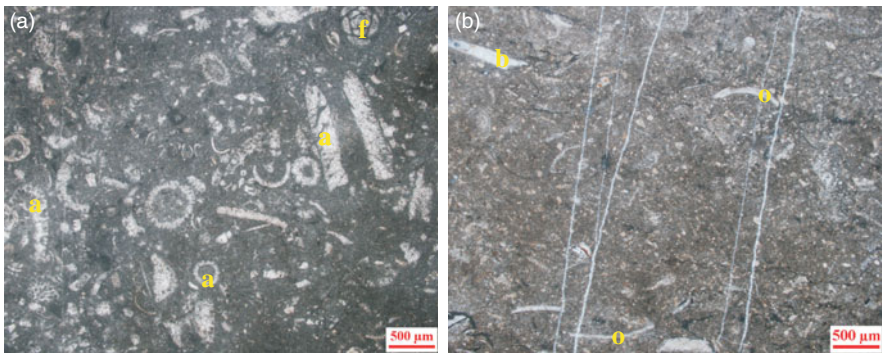

Fig. 9. (Colour online) The microfacies from the EML02 and EML01 limestones in the studied section. XPL – cross-polarized light. (a) Bioclastic packstone with common algae sections (a) and rare foraminifera (f) (sample EML02-3-2). (b) Ostracod mudstone/wackestone with ostracods (o) and bivalve fragments (b) (sample EML01-3-2).

4.b.1. MF2: Bioclastic packstone

In this microfacies, carbonate grains represent ~50 % of the rock and are dominated by algae fragments, such as Dasycladaceae, Udoteaceae and Gymnocodiaceae, together with rare foraminifera and other fragments of invertebrate organisms. Intergranular pores are filled with carbonate mud (Fig. 9a).

4.b.2. MF1: Ostracod mudstone/wackestone

This microfacies is dominated by low-diversity bioclasts, including ostracods and bivalve fragments, occupying ~10 % of the rock (Fig. 9b).

5. Discussion

5.a. Palaeosol interpretation and comparison

5.a.1. Environment of palaeosol formation

Dark grey colours, generally in association with fossil plant accumulations, coal levels, pseudomorphs after pyrite and iron-oxide mottles in the two palaeosols are characteristics of locally reducing or mixed redox conditions (Kraus & Aslan, 1993; Sheldon, 2005; De la Horra *et al.* 2012). The studied palaeosols, interbedded with marine limestones, are considered to have developed in coastal environments. Similar morphological features and mineral compositions are also presented in palaeosols from Middle Permian strata of the SE Iberian Ranges, Spain (De la Horra *et al.* 2012), the Pennsylvanian Paganzo Group of the Paganzo and Río Blanco basins of NW Argentina (Gulbranson *et al.* 2015) and Lower Permian strata in north-central Texas (Tabor & Montañez, 2004), and are interpreted as having formed in poorly drained, shallow depressions on the regionally extensive coastal plain or in coastal environments (Gulbranson *et al.* 2010, 2015).

The higher SiO_2 contents in both palaeosol profiles compared to that in the underlying limestone may be due to detrital quartz introduced into intertidal sedimentary environments. The increase of Cu, Nb and Ni concentrations in the palaeosols relative to the underlying limestones is likely due to the precipitation of these elements within the palaeosols resulting from the higher contents in the parent shales and mudstones and weathering of the overlying basalts (Wang *et al.* 2009, 2011; Mo & Li, 2015). The minor variation in Ti/Al values occurring in the examined palaeosols suggests that there was no change in the sediment source.

5.a.2. Palaeosol interpretation

The pedogenic features and properties of the two studied palaeosols between the Maokou Formation and Emeishan basalts can be correlated with modern acid-sulfate soils developed in coastal environments, e.g. concerning the presence of characteristic minerals such as pyrite and gypsum (Figs 4, 5, 6, 7) and high TS content (Fig. 6).

Abundant pyrite occurs in the Bg horizons of both studied palaeosols (Fig. 4f, g), with framboidal pyrite present (Fig. 5c). Distinct pyrite peaks were determined using XRD (Fig. 8). The presence of pyrite is a key indicator of acid-sulfate soils (van Breemen, 1982; IUSS Working Group WRB, 2006; Fanning *et al.* 2010). XRD-detected gypsum in the studied palaeosols is also commonly documented within acid-sulfate soils (Carson *et al.* 1982; Doner & Lynn, 1989; Ritsema & Groenenberg, 1993; Jennings & Driese, 2014).

The palaeosol sulfur content features are analogous to modern acid-sulfate soils (Boman *et al.* 2008; Gröger *et al.* 2011; Jayalath *et al.* 2016). The studied palaeosols have a typical organic matter profile characterized by higher contents in the top horizon and lower contents in the substratum. The values are generally lower than those of corresponding modern soils, perhaps owing to biotic decomposition or burial dissolution (Krull & Retallack, 2000; Retallack, 2001). However, the carbonized remnants of organic material are observed in the soil matrix and voids (Fig. 5). The highest percentage of TS appears in the Bg horizons of both palaeosols. Sulfate is produced when pyrite undergoes oxidation on soil exposure to the atmosphere. Pyrite oxidation is also accompanied by free sulfuric acid production causing high acidity (van Breemen, 1982; Ritsema & Groenenberg, 1993; Kawahigashi *et al.* 2008; Jayalath *et al.* 2016).

Typically, modern acid-sulfate soils include low pH values between 3 and 5, pyrite concentrations and yellow mottles on ped surfaces or in the soil matrix (van Breemen, 1982; Wilson *et al.* 1999; Fitzpatrick, 2003; IUSS Working Group WRB, 2006; Fitzpatrick *et al.* 2009). Although pH measurement in ancient palaeosols cannot reveal the genuine (prior to burial) values, it is assumed that the Bg horizons in the Qingyin palaeosols would be strongly acidic because of the pyrite and high sulfur content (Dent & Pons, 1995). Ancient acid-sulfate soils show a relatively low Fe content (Fig. 7), with a maximal value in the A horizon. Periodic fluctuations of the water table characteristic for these soils may have caused Fe leaching (Fanning & Fanning, 1989; Golez & Kyuma, 1997). The increase of Al_2O_3, K_2O and Mn

https://doi.org/10.1017/S0016756819001481 Published online by Cambridge University Press

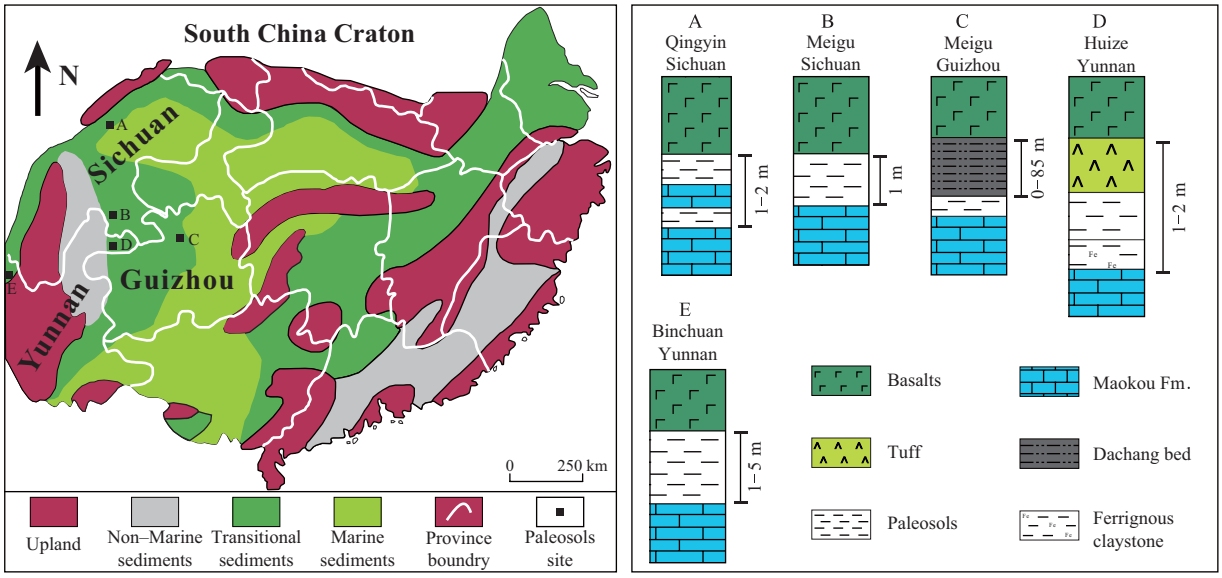

Fig. 10. (Colour online) (a) Palaeoenvironment and distribution of palaeoweathering surfaces and palaeosols in SW China modified from Dai *et al.* (2016) and He *et al.* (2006). (b) Stratigraphic variation of five representative sedimentary successions.

with depth can be attributed to oxidation of the pyrite in the Bg horizons (Shamshuddin *et al.* 2004) because the mobility of Al, Ni, Cu and other potentially toxic metals gradually strengthens as soil acidification is enhanced (Shotyk, 1992; Golez & Kyuma, 1997; Åström, 1998; Sohlenius & Öborn, 2004; Nordmyr *et al.* 2008). Ba/Sr ratio values higher than 2 in the EML02 palaeosol also indicate that the soils formed under acidic conditions (Retallack, 2001).

Jarosite mottles and nodules are not found in the palaeosols in our study, in contrast to the Upper Cretaceous and Paleocene acid-sulfate palaeosols in the USA (McSweeney & Fastovsky, 1987; Retallack, 1994). Our acid-sulfate palaeosols rather resemble soils in the humid tropical climate of Indonesia (Konsten *et al.* 1994), Malaysia (Muhrizal *et al.* 2006) and Vietnam (Kawahigashi *et al.* 2008), which do not contain jarosite. Jarosite nodules were not found in Texas either (Jennings & Driese, 2014). The absence of mottles in the studied palaeosols is possibly attributed to: (1) strongly reducing conditions in the case of the palaeosol formation (e.g. abundant organic matter) unfavourable for the persistence or formation of jarosite (Konsten *et al.* 1994; Michael *et al.* 2015), and (2) the higher dissolution rate of jarosite (Chu *et al.* 2006; Jennings & Driese, 2014), and/or (3) the formation of ferrous sulfate other than jarosite in the case that pyrite was oxidized owing to the low redox potential from the organic matter in the sulfuric horizon (Husson *et al.* 2000; Muhrizal *et al.* 2006). In light of the physical properties in combination with the mineralogical and geochemical features, the palaeosols are considered comparable with modern acid-sulfate soils (Husson *et al.* 2000; Powell & Martens, 2005; Kawahigashi *et al.* 2008).

Significant amounts of carbonates (e.g. calcite) in acid-sulfate soils are rarely present in the humid tropics, because soil formation is affected by acidic water and non-calcareous sediments from the catchment (Pons & van Breemen, 1982; Ritsema & Groenenberg, 1993). However, carbonates were detected in the Bg horizon of the EML01 palaeosol (Figs 6, 8), which formed in the palaeo-equatorial zone (Fig. 2b). It is supposed that calcite in this horizon is inherited from the limestone. Micromorphologically, uniform-sized, rounded calcite fragments were observed in the Bg horizon (Fig. 5e). These are distinct from pedogenic carbonates, which commonly show a mixture of calcite with phyllosilicates, quartz and other minerals, and have various sizes and forms, e.g. fracture fillings or brecciated fragments (Khormali *et al.* 2006; Wanas & Abu El-Hassan, 2006; Cleveland *et al.* 2008; Robins *et al.* 2015).

5.b. Upper Middle Permian palaeosol distribution in SW China

The palaeosols observed at Qingyin, Emeishan, are not the only examples at the boundary between the overlying Emeishan basalts and the limestone of the Maokou Formation. Clay-rich palaeoweathering sequences on the Maokou Formation overlain by Emeishan basalts have been reported in Guizhou, Sichuan and Yunnan provinces of SW China (He *et al.* 2003, 2010) (Fig. 10), but were restricted to the Upper Yangtze Craton, and not observed in the lower Yangtze and South China Block (He *et al.* 2003). The palaeoweathering transition zones vary in thickness from 1 to 5 m (Fig. 10b), and are generally composed of pyrite-bearing claystone, thin layers of coal and siliceous rocks, analogous to the palaeosol sequence observed at Qingyin in the SW Sichuan Basin (He *et al.* 2003, 2010; Lai *et al.* 2008; Sun *et al.* 2010). Furthermore, those coal-forming and root trace-bearing materials in the palaeosols might be considered to be marine mangrove-like plants (Shao *et al.* 1998), which are integral and active components of the coastal landscape (McKee *et al.* 2007) and key indicators of plant growth in acid-sulfate soils (Nguyen *et al.* 2000). Pyrite-bearing claystone derived from the deposition of intertidal sediments (Lin & Melville, 1992, 1993; Ritsema & Groenenberg, 1993) can form rapidly in coastal sedimentary settings owing to the reaction between sulfides and iron oxyhydroxides (Fanning *et al.* 2002). These palaeoweathering crusts situated in the southwest of the Yangtze Plate, which were situated in the eastern palaeo-Tethys around the equator during Middle–Late Permian times (Wang & Jin, 2000) (Fig. 1a), are also classified as acid-sulfate palaeosols. This is because most of the acid-sulfate soils formed within estuaries, swamps, and coastal and river plains

https://doi.org/10.1017/S0016756819001481 Published online by Cambridge University Press

near the equator or in tropical and subtropical regions owing to the waterlogged conditions from the interaction of seawater and abundant organic material (Dent, 1992; Fitzpatrick, 2003), with the morphological and mineralogical properties mentioned above. Claystone and palaeoweathering features, as well as roughly correlative coastal acid-sulfate soils, all in the interval between the Maokou limestone and basalt (Fig. 10), likely manifest a widespread regional palaeopedological phenomenon in the Upper Yangtze Craton.

5.c. Sea-level fluctuations and depositional environment changes in SW China

5.c.1. Relative sea-level indicated by palaeosols

Palaeopedological analysis allows us to reveal the connection of the palaeosols with the relative sea-level changes in the SW Sichuan Basin. Two distinct acid-sulfate palaeosols, separated by a thin limestone bed at Qingyin, and comparable weathered claystone facies were widespread in the Upper Yangtze Craton (Fig. 10). Acid-sulfate soils generally form in intertidal conditions where sources of sulfates, iron and other salts originate from seawater and estuarine sediments, which are within less than 5 m above sea-level and 0.5–1.5 m below sea-level in coastal regions (Walker, 1972; Lin & Melville, 1993; Fitzpatrick, 2003; Powell & Martens, 2005). For example, modern acid-sulfate soils in SE Queensland, Australia, generally occur 1.5 m below sea-level, whereas in Central Queensland, where tides are much higher, acid-sulfate soils are common in coastal plain landscapes of less than 5 m elevation (Ross, 2002). From the perspective of palaeopedology, the palaeosols and their fossil tree stumps imply subaerial exposure. Thus, acid-sulfate palaeosols reveal a fall of relative sea-level from the underlying marine limestones, which is consistent with the normal regression in sequence stratigraphy (Emery & Myers, 1996; Catuneanu, 2002, 2019).

It can be assumed that the elevation in the Qingyin area at the time when these palaeosols were formed was between 5 m above sea-level and 0.5–1.5 m below sea-level. In a broader geographic perspective, similar acid-sulfate palaeosols across SW China may serve as a potential relative sea-level marker, which can outline the boundary between the land and ocean, and indicate the extent of sea coverage at that time in situations when other credible evidence is lacking.

5.c.2. Relative sea-level revealed by the limestone

High-resolution microfacies analysis can give us an insight into the depositional environments and water depth changes in the SW Sichuan Basin.

5.c.2.1. MF2: Bioclastic packstone. The relatively well-preserved bioclasts indicate that these grains are *in situ*, indicating an autochthonous depositional environment. Benthic calcified calcareous algae of Dasycladaceae, Udoteaceae and Gymnocodiaceae grow in tropical and subtropical environments with normal salinity, warm, shallow water (Flügel, 2010). Considering the relative high fossil diversity and content as well as the micritic matrix, the limestone microfacies of EML02 represents a low-energy, shallow-marine carbonate platform sheltered from wave action (Flügel, 2010). Dasycladalean algae extend to depths of 5–6 m below the low-tide level, but can extend down to 12 m in shallow-marine environments (Johnson, 1961; Wray, 1977). Dasycladalean and udoteacean algae of Cenozoic sediments are indicative of a depth of 10–12 m below low-tide level, but are found at a depth of 25 m on rare occasions (Humane & Kundal, 2005; Kundal & Humane, 2007; Kundal, 2010, 2014). Gymnocodiacean algae likely have a wider palaeodepth (Flügel, 2010); however, together with Dasycladalean and Udoteacean algae, this microfacies could have been deposited at shallow palaeodepths of 5–12 m, and likely no more than 25 m.

5.c.2.2. MF1: Ostracod mudstone/wackestone. The MF1 is characterized by very low bio-diversity and poorly preserved fossils, mainly including ostracods and bivalves, which is in contrast with the MF2 bioclastic packstone, representing EML01-3. Compared with the MF2, the MF1 indicates an intertidal, or even supratidal, environment above the low-tide level, and a more restricted and shallower environment with abnormal water circulation and salinity. Such an environment suggests an intertidal water depth of no more than 10 m depending on the tide (Flügel, 2010).

5.c.3. Sea-level fluctuations and depositional environment changes in SW China

Sea-level is recorded by two acid-sulfate palaeosols and two beds of limestone at Qingyin in the SW Sichuan Basin. The relative sea-level variations can be estimated by the palaeosol and limestone sequences. The magnitude of relative sea-level fall is less than 6.5 m based on the development of acid-sulfate soils, whereas the relative sea-level rise is close to the surface and usually less than 10 m, as suggested by the deposition of the thin limestone. The topmost limestone of the Maokou Formation suggests a shallow-marine environment with a depth of 5–25 m, and therefore the amplitudes of relative sea-level fluctuations range from 0 to a maximum of 25 m in late Middle Permian times of the Sichuan Basin in SW China, which is within the range of previous research examining the global sedimentary record (Ross & Ross, 1995; Haq & Schutter, 2008; Rygel *et al.* 2008). Correspondingly, the depositional environment shifted from shallow-marine to intertidal or even supratidal facies, and subsequently to tidal-flat facies, ultimately with littoral to continental volcanic facies during late Middle Permian times (Fig. 11).

From the view of sequence stratigraphy, the progradational pattern of the facies does not mean the fall of relative sea-level, and actually may be a forced regression; in that case the sea-level is probably rising (Emery & Myers, 1996; Catuneanu, 2002, 2019). The acid-sulfate palaeosol facies on top of the marine limestone in the studied areas certainly reveal marine regression events. But the marine regression, in this case, is possibly produced by a fall of relative sea-level or a forced regression.

As the relative sea-level is falling, the emerged seafloor is exposed to erosional processes (truncation) and incision by fluvial systems. Besides the acid-sulfate palaeosols at Qingyin, the palaeosol-like sequences (palaeoweathering crusts) (He *et al.* 2003; Lai *et al.* 2008; Sun *et al.* 2010) and palaeokarsts (He *et al.* 2010), formed under aerial or subaerial conditions on the Maokou Formation and overlain by the Emeishan basalts, ranged in thickness from 1 to 5 m and are distributed widely in Guizhou, Sichuan and Yunnan provinces of SW China. The presence of extensively developed palaeosols and palaeokarsts with a thickness of less than 5 m that occurred during <2 Ma years (~262–260 Ma) in SW China definitely reveals that the submerged seafloor is exposed, weathered and eroded.

The sedimentary hiatuses marked by these palaeosols and palaeokarsts illustrate that the rate of sediment supply is less than the rate of sediment accommodation at the shoreline, and the marine regressions indicated by the palaeosols are the normal

https://doi.org/10.1017/S0016756819001481 Published online by Cambridge University Press

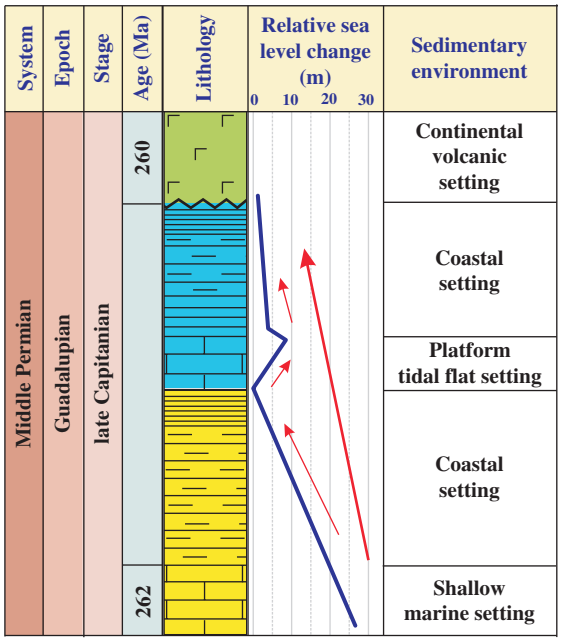

Fig. 11. (Colour online) Chronostratigraphic column of the SW Sichuan Basin showing the change in relative sea-level and depositional environments. Shallow-marine setting is as identified in Lai *et al.* (2008) and continental volcanic setting is derived from He *et al.* (2003). The blue line refers to the relative sea-level change fluctuation curve and the red line represents the trend line of relative sea-level change.

regression (i.e. fall of relative sea-level) rather than a forced regression in sequence stratigraphy (Emery & Myers, 1996; Catuneanu, 2002, 2019).

Two marine regressions, i.e. the ~0–18.5 m and ~3.5 m fall of sea-level, were respectively inferred in SW China for late Middle Permian times (~262–260 Ma) (Fig. 11). Ross & Ross (1995) suggested that the amplitudes of the sea-level fluctuations ranged between 10 and 100 m in South China during Capitanian times according to the third-order depositional sequences of the Permian. Furthermore, the short-term sea-level fluctuations were not more than 75 m on a global scale in Capitanian times (~265.8–260.4 Ma) according to the seismostratigraphic and sedimentological data. In addition, Lai *et al.* (2008) reported that the sedimentary environment of the Mudstone Unit of the Maokou Formation in northern Sichuan, which is time-equivalent with the interval between the Maokou Formation and Emeishan basalts in the present study, was an extremely shallow-water setting, such as a lagoon/tidal-flat environment. However, our results are somewhat different from those estimated by Isozaki *et al.* (2008) and Saitoh *et al.* (2013), who postulated depths of over 150 m in northern Sichuan, using different methods.

5.d. Implications for sea-level changes in SW China in late Middle Permian times

Sea-level fluctuations during Capitanian times in SW China, situated in the eastern palaeo-Tethys, were characterized by short-term regression–transgression events associated with a long-term global marine regression in Capitanian times. The long-term regression resulted in the substantial sea-level drop at the Middle–Late Permian boundary (Fig. 12), which is clearly recorded by an extensive unconformity in South China and by termination of the thick reef complex in SW North America (Ross & Ross, 1995; Hallam & Wignall, 1999; Tong *et al.* 1999; Jin *et al.* 2006; Haq & Schutter, 2008; Kofukuda *et al.* 2014; Bhattacharya & Banerjee, 2015).

Some workers have provided estimates of the amplitude of sea-level changes in northern Sichuan thus far. Isozaki *et al.* (2008) and Saitoh *et al.* (2013) reported that sea-level rose significantly in two steps, resulting in change of the sedimentary environment from a euphotic shelf (generally shallower than 150 m) to a disphotic slope/basin (a depth of between 150 and 250 m) in Capitanian times (Saitoh *et al.* 2014) based on the stratigraphic changes in litho- and bio-facies in northern Sichuan (Fig. 12). Qiu *et al.* (2014*b*) reported that the sea-level variations in the Laibin area of Guangxi during Capitanian times were within the transition zone between the lower slope and platform margin according to the sedimentary facies analysis (Fig. 12). However, the palaeopedological results presented here suggest that sea-level initially dropped by up to 6.5 m, followed by a rise of up to 10 m, and again dropped within the scope of 6.5 m in late Capitanian times (~262–260 Ma). Overall, our results suggest that the short-term variations in sea-level in SW China were consistent with the long-term decline on a global scale (Fig. 12).

Long-term sea-level variations are thought to be driven largely by slow tectonic processes that influence the volumetric capacity of the ocean basins, whereas short-term changes may be attributed to glaciation (Haq & Schutter, 2008). Moreover, Isozaki (2009*a*) suggested that mantle superplume activity was likely responsible for the global-scale sea-level drop around the Guadalupian/Lopingian boundary. In this study, the sea-level fluctuations in Capitanian times are possibly linked to global climatic fluctuations and regional tectonic activities (Isozaki, 2006; Isozaki *et al.* 2007, 2008, 2011). The global cooling episode in late Middle Permian times coupled with the Kamura event, a unique oceanographic event, occurred in the mid-superocean (Isozaki, 2006; Isozaki *et al.* 2007, 2011; Fielding *et al.* 2008; Isozaki & Aljinović, 2009; Fujimoto *et al.* 2012). In particular, a relatively cool climate prevailed in the tropical domain (Isozaki, 2009*b*; Isozaki & Aljinović, 2009) and resulted in seawater from the oceans evaporating and then snowing onto high elevation continental ice (Kofukuda *et al.* 2014). Thus, global cooling may have caused a global regression that influenced South China. In addition, the palaeokarst on top of the Maokou Formation, including palaeokarst relief, sinkholes, caves and tower karst, are geomorphological evidence of a tropical climate in SW China (Guizhou, Sichuan and Yunnan; He *et al.* 2003, 2010). Meanwhile, marine deposits covering the palaeokarst were also recorded in Guizhou and Sichuan provinces of SW China (He *et al.* 2006). A regressive and transgressive phase is associated with regional basin uplift or depression. A regional tectonic uplift (i.e. the 'Dongwu Movement') in most of the South China Block occurred in latest Middle Permian times (Hu, 1994; Editing Committee of Stratigraphy, 2000), which may have been related to the Emeishan basalts (He *et al.* 2005), and might have contributed to the exposure of the regressive carbonate platform and the karst and palaeosol formation. Furthermore, soil formation, burial and erosion are usually related to changes in tectonic and climatic conditions (Muhs & Bettis, 2003; Retallack, 2008). Therefore, the formation of acid-sulfate palaeosol–limestone sequences may have been a result of sea-level changes linked to the global climatic conditions and regional tectonic activities in late Middle Permian times.

In the present study, the joint analysis of coastal plain palaeosols and carbonate microfacies offers a tool for estimating relative sea-level changes or water depths, which can help to detect

https://doi.org/10.1017/S0016756819001481 Published online by Cambridge University Press

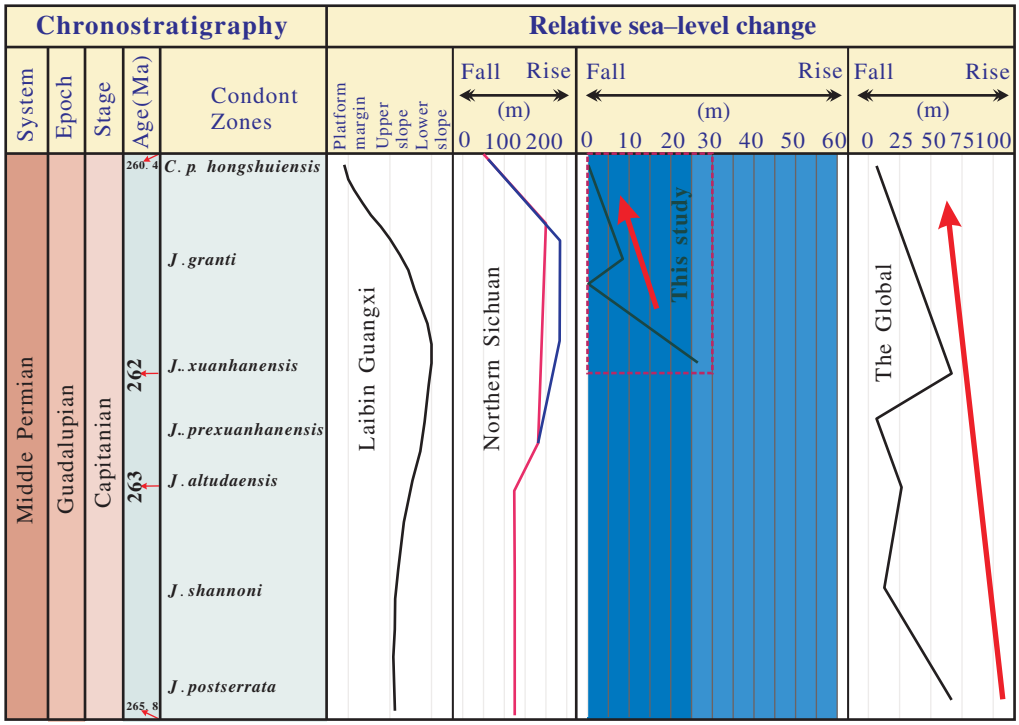

Fig. 12. (Colour online) Reconstructed sea-level curve for SW China and the world showing the relative sea-level changes during Capitanian time. The conodont zones are derived from Qiu *et al.* (2014*b*) and the timescale is modelled after Wardlaw *et al.* (2004). The sea-level curve for Laibin, Guangxi, is from Qiu *et al.* (2014*b*), the pink and blue lines for northern Sichuan are from Isozaki *et al.* (2008) and Saitoh *et al.* (2013), and the global curve is from Haq & Schutter (2008). Dark blue boxes are common sea-level change magnitude values; light blue boxes represent the size of rare events of Rygel *et al.* (2008).

multiple and small-scale variations in the sea-level. Coastal acid-sulfate soils overlying marine sediments are widely distributed in tropical or subtropical zones, such as in Indonesia (Konsten *et al.* 1994), Malaysia (Muhrizal *et al.* 2006) and Vietnam (Kawahigashi *et al.* 2008), and this specific kind of soil has been reported from other geological periods (Kraus, 1998). Palaeopedology combined with carbonate microfacies analysis may therefore be used to determine sea-level changes over geological time.

6. Conclusions

In the SW Sichuan Basin, a section composed of two palaeosols separated by a 20 cm thick limestone was observed from the contact between the Maokou Formation and Emeishan basalts. Integration of pedological analysis based on micromorphological, morphological, mineralogical and geochemical properties and sedimentological analysis based on carbonate microfacies determination revealed that the studied palaeosols have developed as acid-sulfate soils in a coastal setting with subaerial exposure like modern acid-sulfate soils. Comparable sedimentary facies with acid-sulfate palaeosols are widespread in the Upper Yangtze Craton of South China and outline a large region of intertidal palaeoenvironments. The palaeosol–limestone alternation is also evidence of relative sea-level fluctuations. The depositional environment experienced a series of changes from shallow-marine to littoral, followed by tidal-flat and back to littoral. These depositional environments were overlain by continental basalts in late Capitanian times.

The magnitude of relative sea-level fluctuations likely ranged from 0 to 25 m, judging from the relationship between the acid-sulfate-soil-like palaeosols and carbonate microfacies. Marine regression was likely related to the global cooling episode and regional tectonic uplift. A short transgression within late Capitanian times recorded within the thin limestone underlying the coal-bearing shale was not reported in the other areas of South China, but marked a major environmental change in SW China. It may be related to localized depression caused by mantle plume-related substantial uplift and erosion activity in SW China. Hence, we speculate that global cooling caused the long-term Capitanian marine regression, aided by uplift of the Sichuan Basin during late Middle Permian times. We propose that the sequence of coastal acid-sulfate soils overlying limestone can provide a new tool for the estimation of sea-level fluctuations.

Acknowledgements. This study was funded by the National Natural Science Foundation of China (Grant Nos. 41771248 and 41371225) and the National Basic Research Program of China (Grant No. 2012CB822003). The authors would like to thank two anonymous reviewers for their valuable and detailed comments and suggestions.

References

Adatte T, Keller G and Stinnesbeck W (2002) Late Cretaceous to early Paleocene climate and sea-level fluctuations: the Tunisian record. *Palaeogeography, Palaeoclimatology, Palaeoecology* **178**, 165–96.

Ali JR, Lo CH, Thompson GM and Song X (2004) Emeishan basalt Ar–Ar overprint ages define several tectonic events that affected the western Yangtze platform in the Mesozoic and Cenozoic. *Journal of Asian Earth Sciences* **23**, 163–78.

Ali JR, Thompson GM, Zhou MF and Song X (2005) Emeishan large igneous province, SW China. *Lithos* **79**, 475–89.

Álvaro JJ, Vliet-Lanoë BV, Vennin E and Blanc-Valleron MM (2003) Lower Cambrian paleosols from the Cantabrian Mountains (northern Spain): a comparison with Neogene–Quaternary estuarine analogues. *Sedimentary Geology* **163**, 67–84.

https://doi.org/10.1017/S0016756819001481 Published online by Cambridge University Press

Åström M (1998) Mobility of Al, P and alkali and alkaline earth metals in acid sulphate soils in Finland. *Science of the Total Environment* **215**, 19–30.

Bak YS (2015) Mid-Holocene sea-level fluctuation inferred from diatom analysis from sediments on the west coast of Korea. *Quaternary International* **384**, 139–44.

Beiranvand B, Ghasemi-Nejad E and Kamali MR (2013) Palynomorphs' response to sea-level fluctuations: a case study from Late Cretaceous–Paleocene, Gurpi Formation, SW Iran. *Journal Geopersia* **3**, 11–24.

Bhattacharya B and Banerjee PP (2015) Record of Permian Tethyan transgression in Eastern India: a reappraisal of the Barren Measures Formation, West Bokaro Coalfield. *Marine and Petroleum Geology* **67**, 170–9.

Blakey RC (2007) Carboniferous–Permian paleogeography of the assembly of Pangaea. In *Proceedings of the XVth International Congress on Carboniferous and Permian Stratigraphy* (ed. TE Wong), pp. 443–56. Amsterdam: Royal Dutch Academy of Arts and Sciences.

Boman A, Åström M and Fröjdö S (2008) Sulfur dynamics in boreal acid sulfate soils rich in metastable iron sulfide—the role of artificial drainage. *Chemical Geology* **255**, 68–77.

Bond DPG and Wignall PB (2009) Latitudinal selectivity of foraminifer extinctions during the late Guadalupian crisis. *Paleobiology* **35**, 465–83.

Brain MJ, Kemp AC, Horton BP, Culver SJ, Parnell AC and Cahill N (2015) Quantifying the contribution of sediment compaction to late Holocene salt-marsh sea-level reconstructions (North Carolina, USA). *Quaternary Research* **83**, 41–51.

Brett CE and Mclaughlin PI (2009) Response of shallow marine biotas to sea-level fluctuations: a review of faunal replacement and the process of habitat tracking. *Paleobiology* **22**, 228–44.

Bullock P, Fedoroff N, Jongerius A, Stoops G, Tursina T and Babel U (1985) *Handbook for Soil Thin Section Description*. Albrighton: Waine Research Publications, 152 pp.

Bureau of Geology and Mineral Resources of Sichuan Province (1991) *Regional Geology of Sichuan Province*. Beijing: Geological Publishing House, pp. 443–56 (in Chinese).

Camoin GF and Webster JM (2015) Coral reef response to Quaternary sea-level and environmental changes: state of the science. *Sedimentology* **62**, 401–28.

Carson CD, Fanning DS and Dixon CJ (1982) Alfisols and Ultisols with acid sulfate weathering features in Texas. In *Acid Sulfate Weathering* (ed. JA Kittrick), pp. 127–46. SSSA Special Publication 10. Madison: Soil Science Society of America.

Catuneanu O (2002) Sequence stratigraphy of clastic systems: concepts, merits, and pitfalls. *Journal of African Earth Sciences* **35**, 1–43.

Catuneanu O (2019) Model-independent sequence stratigraphy. *Earth-Science Reviews* **188**, 312–88.

Chen ZQ, Jin Y and Shi GR (1998) Permian transgression-regression sequences and sea-level changes of South China. *Proceedings of the Royal Society of Victoria* **110**, 345–67.

Chu CX, Lin CX, Wu YG, Lu WZ and Long J (2006) Organic matter increases jarosite dissolution in acid sulfate soils under inundation conditions. *Australian Journal of Soil Research* **44**, 11–16.

Cleveland DM, Nordt LC and Atchley SC (2008) Paleosols, trace fossils, and precipitation estimates of the uppermost Triassic strata in northern New Mexico. *Palaeogeography, Palaeoclimatology, Palaeoecology* **257**, 421–44.

Dai SF, Chekryzhov IY, Seredin VV, Nechaev VP, Graham IT, Hower JC, Ward CR, Ren DY and Wang XB (2016) Metalliferous coal deposits in East Asia (primorye of Russia and South China): a review of geodynamic controls and styles of mineralization. *Gondwana Research* **29**, 60–82.

De la Horra R, Galán-Abellán AB, López-Gómez J, Sheldon ND, Barrenechea JF, Luque FJ, Arche A and Benito MI (2012) Paleoecological and paleoenvironmental changes during the continental Middle–Late Permian transition at the SE Iberian Ranges, Spain. *Global and Planetary Change* **94–95**, 46–61.

Dent D (1992) Reclamation of acid sulphate soils. *Advances in Soil Science* **17**, 79–122.

Dent DL and Pons LJ (1995) A world perspective on acid sulphate soils. *Geoderma* **67**, 263–76.

Doner HE and Lynn WC (1989) Carbonates, halite, sulfate, and sulfide minerals. In *Minerals in Soil Environments* (eds JB Dixon and SB Weed), pp. 279–330. Madison: Soil Science Society of America.

Dreimanis A (1962) Quantitative gasometric determinations of calcite and dolomite by using Chittick apparatus. *Journal of Sedimentary Petrology* **32**, 520–9.

Dunham RJ (1962) Classification of carbonate rocks according to depositional textures. *American Association of Petroleum Geologists* **1**, 108–21.

Editing Committee of Stratigraphy (2000) *Permian in China*. Beijing: Geological Publishing House, pp. 443–56 (in Chinese with English abstract).

Emery D and Myers KJ (1996) *Sequence Stratigraphy*. Oxford: Blackwell, 304 pp.

Fanning DS and Fanning MCB (1989) *Soil: Morphology, Genesis, and Classification*, pp. 443–56. New York: John Wiley and Sons.

Fanning DS, Rabenhorst MC, Balduff DM, Wagner DP, Orr RS and Zurheide PK (2010) An acid sulfate perspective on landscape/seascape soil mineralogy in the US Mid-Atlantic region. *Geoderma* **154**, 457–64.

Fanning DS, Rabenhorst MC, Burch SN, Islam KR and Tangren SA (2002) Sulfides and sulfates. In *Soil Mineralogy with Environmental Application* (eds JB Dixon and DG Schulze), pp. 229–60. Madison: Soil Science Society of America.

Fielding CR, Frank TD and Isbell JL (eds) (2008) *Resolving the Late Paleozoic Ice Age in Time and Space*. Geological Society of America, Special Paper no. 441, 354 pp.

Fitzpatrick RW (2003) Overview of acid sulfate soil properties, environmental hazards, risk mapping and policy development in Australia. In *Advances in Regolith* (ed. IC Roach), pp. 122–25. Canberra: CRCLEME.

Fitzpatrick RW, Shand P and Merry RH (2009) Acid sulfate soils. In *Natural History of the Riverland and Murraylands* (ed. JT Jennings), pp. 65–111. Adelaide: Royal Society of South Australia.

Flügel E (2010) *Microfacies of Carbonate Rocks: Analysis, Interpretation and Application*, 2nd Edition, pp. 7–266. Berlin: Springer-Verlag.

Fu JY, Ding ZH, Wu YM and Lin HN (2007) Determination of high-sulfur content environmental samples by spectroscopic barium turbidity method. *Journal of Xiamen University (Natural Science)* **46**, 880–3 (in Chinese with English abstract).

Fujimoto T, Otoh S, Orihashi Y, Hirata T, Yokoyama TD, Shimojo M, Kouchi Y, Obara H, Ishizaki Y, Tsukada K, Kurihara T, Manchuk N and Sersmaa G (2012) Permian peri-glacial deposits from central Mongolia in central Asian orogenic belt: a possible indicator of the Capitanian cooling event. *Resource Geology* **62**, 408–22.

Galeotti S and Coccioni R (2002) Changes in coiling direction of *Cibicidoides pseudoacutus* (Nakkady) across the Cretaceous–Tertiary transition of Tunisia: paleoecological and biostratigraphic implications. *Palaeogeography, Palaeoclimatology, Palaeoecology* **178**, 197–210.

Girone A (2005) Response of otolith assemblages to sea-level fluctuations at the lower Pleistocene Montalbano Jonico section (southern Italy). *Bollettino Della Societa Paleontologica Italiana* **44**, 35–45.

Goldstein RH and Franseen EK (1995) Pinning points: a method providing quantitative constraints on relative sea-level history. *Sedimentary Geology* **95**, 1–10.

Golez NV and Kyuma K (1997) Influence of pyrite oxidation and soil acidification on some essential nutrient elements. *Aquacultural Engineering* **16**, 107–24.

Gröger J, Proske U, Hanebuth TJ and Hamer K (2011) Cycling of trace metals and rare earth elements (REE) in acid sulfate soils in the Plain of Reeds, Vietnam. *Chemical Geology* **288**, 162–77.

Gulbranson EL, Montañez IP, Schmitz MD, Limarino CO, Isbell JL, Marenssi SA and Crowley JL (2010) High-precision U–Pb calibration of Carboniferous glaciation and climate history, Paganzo Group, NW Argentina. *Geological Society of America Bulletin* **122**, 1480–98.

Gulbranson EL, Montañez IP, Tabor NJ and Limarino CO (2015) Late Pennsylvanian aridification on the southwestern margin of Gondwana (Paganzo Basin, NW Argentina): a regional expression of a global climate perturbation. *Palaeogeography, Palaeoclimatology, Palaeoecology* **417**, 220–35.

https://doi.org/10.1017/S0016756819001481 Published online by Cambridge University Press

Gvirtzman G, Martinotti GM and Moshkovitz S (1997) Stratigraphy of the Plio-Pleistocene sequence of the Mediterranean coastal belt of Israel and its implications for the evolution of the Nile cone. In *The Pleistocene Boundary and the Beginning of the Quaternary* (ed. JA Van Couvering), pp. 156–68. Cambridge: Cambridge University Press.

Hallam A and Wignall P (1999) Mass extinctions and sea-level changes. *Earth-Science Reviews* **48**, 217–50.

Han Z, Hu XM, Li J and Garzanti E (2016) Jurassic carbonate microfacies and relative sea-level changes in the Tethys Himalaya (southern Tibet). *Palaeogeography, Palaeoclimatology, Palaeoecology* **456**, 1–20.

Haq BU and Schutter SR (2008) A chronology of Paleozoic sea-level changes. *Science* **322**, 64–8.

He B, Xu YG, Chung SL, Xiao L and Wang Y (2003) Sedimentary evidence for a rapid, kilometer-scale crustal doming prior to the eruption of the Emeishan flood basalts. *Earth and Planetary Science Letters* **213**, 391–405.

He B, Xu YG, Guan JP and Zhong YT (2010) Paleokarst on the top of the Maokou Formation: further evidence for domal crustal uplift prior to the Emeishan flood volcanism. *Lithos* **119**, 1–9.

He B, Xu YG, Huang XL, Luo ZY, Shi YR, Yang QJ and Yu SY (2007) Age and duration of the Emeishan flood volcanism, SW China: geochemistry and SHRIMP zircon U–Pb dating of silicic ignimbrites, post-volcanic Xuanwei Formation and clay tuff at the Chaotian section. *Earth and Planetary Science Letters* **255**, 306–23.

He B, Xu YG, Wang YM and Luo ZY (2006) Sedimentation and lithofacies paleogeography in southwestern China before and after the Emeishan flood volcanism: new insights into surface response to mantle plume activity. *Journal of Geology* **114**, 117–32.

He B, Xu YG, Wang YM and Xiao L (2005) Nature of the Dongwu Movement and its temporal and spatial evolution. *Earth Science (Journal of China University of Geosciences)* **30**, 89–96 (in Chinese with English abstract).

Hou ZQ, Chen W and Lu JR (2002) Collision event during 177–135 Ma on the eastern margin of the Qinghai-Tibet plateau: evidence from $^{40}Ar/^{39}Ar$ dating for basalts on the western margin of the Yangtze platform. *Acta Geologica Sinica* **76**, 194–204.

Hu S (1994) On the event of Dongwu Movement and its relation with Permian subdivision. *Journal of Stratigraphy* **18**, 309–15 (in Chinese with English abstract).

Huang H, Cawood PA, Hou MC, Yang JH, Ni SJ, Du YS, Yan ZK and Wang J (2016) Silicic ash beds bracket Emeishan Large Igneous province to < 1 m.y. at ~ 260 Ma. *Lithos* **264**, 17–27.

Humane SK and Kundal P (2005) Halimedacean and Udoteacean algae from the Mid-Tertiary western carbonate platform of the Kachchh, India: possible paleoenvironments and evolution. *Environmental Micropaleontology, Microbiology and Meiobenthology* **2**, 4–27.

Husson O, Verburg PH, Phung MT and Van Mensvoort MEF (2000) Spatial variability of acid sulphate soils in the Plain of Reeds, Mekong delta, Vietnam. *Geoderma* **97**, 1–19.

Isozaki Y (2006) Guadalupian (Middle Permian) giant bivalve Alatoconchidae from a mid-Panthalassan paleo-atoll complex in Kyushu, Japan: a unique community associated with Tethyan fusulines and corals. *Proceedings of the Japan Academy, Series B* **82**, 25–32.

Isozaki Y (2009a) The Illawarra Reversal: the fingerprint of a superplume that triggered Pangean breakup and the end-Guadalupian (Permian) mass extinction. *Gondwana Research* **15**, 421–32.

Isozaki Y (2009b) Integrated "plume winter" scenario for the double-phased extinction during the Paleozoic–Mesozoic transition: the G–LB and P–TB events from a Panthalassan perspective. *Journal of Asian Earth Sciences* **36**, 459–80.

Isozaki Y and Aljinović D (2009) End-Guadalupian extinction of the Permian gigantic bivalve Alatoconchidae: end of gigantism in tropical seas by cooling. *Palaeogeography, Palaeoclimatology, Palaeoecology* **284**, 11–21.

Isozaki Y, Aljinović D and Kawahata H (2011) The Guadalupian (Permian) Kamura event in European Tethys. *Palaeogeography, Palaeoclimatology, Palaeoecology* **308**, 12–21.

Isozaki Y, Kawahata H and Ota A (2007) A unique carbon isotope record across the Guadalupian–Lopingian (Middle–Upper Permian) boundary in mid-oceanic paleo-atoll carbonates: the high-productivity "Kamura event" and its collapse in Panthalassa. *Global and Planetary Change* **55**, 21–38.

Isozaki Y, Yao J, Ji Z, Saitoh M, Kobayashi N and Sakai H (2008) Rapid sea-level change in the Late Guadalupian (Permian) on the Tethyan side of South China: litho-and biostratigraphy of the Chaotian section in Sichuan. *Proceedings of the Japan Academy, Series B* **84**, 344–53.

Isozaki Y, Yao J, Matsuda T, Sakai H, Ji Z, Shimizu N, Kobayashi N, Kawahata H, Nishi H, Takano M and Kubo T (2004) Stratigraphy of the Middle–Upper Permian and lowermost Triassic at Chaotian, Sichuan, China record of Late Permian double mass extinction event. *Proceedings of the Japan Academy, Series B* **80**, 10–16.

IUSS Working Group WRB (2006) *World Reference Base for Soil Resources*, 2nd ed. Rome: Food and Agriculture Organization of the United Nations, 127 pp.

Jank M, Wetzel A and Meyer CA (2006) Late Jurassic sea-level fluctuations in NW Switzerland (late Oxfordian to late Kimmeridgian): closing the gap between the boreal and Tethyan realm in western Europe. *Facies* **52**, 487–519.

Jarvis I, Mabrouk A, Moody RTJ, Murphy AM and Sandman RI (2008) Applications of carbon isotope and elemental (Sr/Ca, Mn) chemostratigraphy to sequence analysis: sea-level change and the global correlation of pelagic carbonates. In *The Geology of East Libya, Vol. 1* (eds MJ Salem and AS El-Hawat) pp. 369–96. Tripoli: Earth Science Society of Libya.

Jayalath N, Mosley LM, Fitzpatrick RW and Marschner P (2016) Addition of organic matter influences pH changes in reduced and oxidised acid sulfate soils. *Geoderma* **262**, 125–32.

Jennings DS and Driese SG (2014) Understanding barite and gypsum precipitation in upland acid-sulfate soils: an example from a Lufkin Series toposequence, south-central Texas, USA. *Sedimentary Geology* **299**, 106–18.

Jin Y and Shang Q (2000) The Permian of China and its interregional correlation. In *Permian–Triassic Evolution of Tethys and Western Circum-Pacific* (eds HF Yin, JM Dickins, GR Shi and JN Tong), pp. 71–98. Developments in Palaeontology and Stratigraphy vol. 18. Amsterdam: Elsevier.

Jin YG, Shen SZ, Henderson CM, Wang XD, Wang W, Wang Y, Cao CQ and Shang QH (2006) The global stratotype section and point (GSSP) for the boundary between the Capitanian and Wuchiapingian stage (Permian). *Episodes* **29**, 253–62.

Johnson JH (1961) *Limestone Building Algae and Algal Limestone*. Golden: Colorado School of Mines, 297 pp.

Kawahigashi M, Do NM, Nguyen VB and Sumida H (2008) Effects of drying on the release of solutes from acid sulfate soils distributed in the Mekong Delta, Vietnam. *Soil Science and Plant Nutrition* **54**, 495–506.

Khormali F, Abtahi A and Stoops G (2006) Micromorphology of calcitic features in highly calcareous soils of Fars Province, Southern Iran. *Geoderma* **132**, 31–46.

Kofukuda D, Isozaki Y and Igo H (2014) A remarkable sea-level drop and relevant biotic responses across the Guadalupian–Lopingian (Permian) boundary in low-latitude mid-Panthalassa: irreversible changes recorded in accreted paleo-atoll limestones in Akasaka and Ishiyama, Japan. *Journal of Asian Earth Sciences* **82**, 47–65.

Konsten CJM, Breemen NV, Suping S, Aribawa IB and Groenenberg JE (1994) Effects of flooding on pH of rice-producing, acid sulfate soils in Indonesia. *Soil Science Society of America Journal* **58**, 871–83.

Kraus MJ (1998) Development of potential acid sulfate paleosols in Paleocene floodplains, Bighorn Basin, Wyoming, USA. *Palaeogeography, Palaeoclimatology, Palaeoecology* **144**, 203–24.

Kraus MJ and Aslan A (1993) Eocene hydromorphic paleosols: significance for interpreting ancient floodplain processes. *Journal of Sedimentary Petrology* **63**, 453–63.

Krull ES and Retallack GJ (2000) $\delta^{13}C$ depth profiles from paleosols across the Permian–Triassic boundary: evidence for methane release. *Geological Society of America Bulletin* **112**, 1459–72.

Kundal P (2010) Biostratigraphic, paleobiogeographic and paleoenvironmental significance of calcareous algae. In *Applied Micropaleontology* (eds P Kundal and SK Humane). *Gondwana Geological Magazine, Special Issue* **25**, 125–32.

Kundal P (2014) Miocene calcareous algae from India: retrospect and prospect. In *Miocene of India* (ed. RP Tiwari), pp. 135–43. Special Publication of the Palaeontology Society of India no. 5.

https://doi.org/10.1017/S0016756819001481 Published online by Cambridge University Press

Kundal P and Humane SK (2007) Chattian and Burdigalian Dasycladacean algae from Kachchh, Western India and their implications on environment of deposition. *Journal of the Geological Society of India* **69**, 788–94.

Lai XL, Wang W, Wignall PB, Bond DPG, Jiang HS, Ali JR and Sun YD (2008) Palaeoenvironmental change during the end-Guadalupian (Permian) mass extinction in Sichuan, China. *Palaeogeography, Palaeoclimatology, Palaeoecology* **269**, 78–93.

Li J, Wen XY and Huang CM (2016) Lower Cretaceous paleosols and paleoclimate in Sichuan Basin, China. *Cretaceous Research* **62**, 154–71.

Lin C and Melville MD (1992) Mangrove soil: a potential contamination source to estuarine ecosystems of Australia. *Wetlands* **11**, 68–75.

Lin C and Melville MD (1993) Control of soil acidification by fluvial sedimentation in an estuarine floodplain, eastern Australia. *Sedimentary Geology* **85**, 271–84.

Ljung K, Maley F, Cook A and Weinstein P (2009) Acid sulfate soils and human health—a millennium ecosystem assessment. *Environment International* **35**, 1234–42.

McKee KL, Cahoon DR and Feller IC (2007) Caribbean mangroves adjust to rising sea level through biotic controls on change in soil elevation. *Global Ecology and Biogeography* **16**, 545–56.

McSweeney K and Fastovsky DE (1987) Micromorphological and SEM analysis of Cretaceous–Paleogene petrosols from eastern Montana and western North Dakota. *Geoderma* **40**, 49–63.

Michael PS, Fitzpatrick R and Reid R (2015) The role of organic matter in ameliorating acid sulfate soils with sulfuric horizons. *Geoderma* **255–256**, 42–9.

Mo GY and Li FD (2015) Geological features of basalt-derived Nb and Ta ore deposits in Weining, Guizhou, China. *Nonferrous Metals Abstract* **30**, 26–8 (in Chinese).

Muhrizal S, Shamshuddin J, Fauziah I and Husni MAH (2006) Changes in iron-poor acid sulfate soil upon submergence. *Geoderma* **131**, 110–22.

Muhs DR and Bettis EAI (2003) Quaternary loess-paleosol sequences as examples of climate-driven sedimentary extremes. *Geological Society of America Special Paper* **370**, 53–74.

Munsell Color (2000) *Munsell Soil Color Charts*. New Windsor, NY: Munsell Color Company.

Narkiewicz M and Retallack GJ (2014) Dolomitic paleosols in the lagoonal tetrapod track-bearing succession of the Holy Cross Mountains (Middle Devonian, Poland). *Sedimentary Geology* **299**, 74–87.

Nguyen VL, Ta TKO and Tateishi M (2000) Late Holocene depositional environments and coastal evolution of the Mekong River Delta, Southern Vietnam. *Journal of Asian Earth Sciences* **18**, 427–39.

Nordmyr L, Åström M and Peltola P (2008) Metal pollution of estuarine sediments caused by leaching of acid sulphate soils. *Estuarine Coastal and Shelf Science* **76**, 141–52.

Olde K, Jarvis I, Uličný D, Pearce MA, Trabucho-Alexandre J, Čech S, Gröcke DR, Laurin J, Švábenická L and Tocher BA (2015) Geochemical and palynological sea-level proxies in hemipelagic sediments: a critical assessment from the Upper Cretaceous of the Czech Republic. *Palaeogeography, Palaeoclimatology, Palaeoecology* **435**, 222–43.

Pons LJ (1973) Outline of genesis, characteristics, classification and improvement of acid sulphate soils. In *Proceedings of the 1972 (Wageningen, Netherlands) International Acid Sulphate Soils Symposium, Volume 1* (ed. H Dost), pp. 3–27. Wageningen: Netherlands: International Institute for Land Reclamation and Improvement Publication no. 18.

Pons LJ and van Breeman N (1982) Factors influencing the formation of potential acidity in tidal swamps. In *Proceedings of the Bangkok Symposium on Acid Sulphate Soils* (eds H Dost and N van Breeman), pp. 37–51. Wageningen, Netherlands: International Institute for Land Reclamation and Improvement Publication no. 31.

Powell B and Martens M (2005) A review of acid sulfate soil impacts, actions and policies that impact on water quality in Great Barrier Reef catchments, including a case study on remediation at East Trinity. *Marine Pollution Bulletin* **51**, 149–64.

Qiu Z, Sun S, Wang Q and Zou C (2014a) Facies and sequence stratigraphy of the global stratotype sections for the boundary between the Guadalupian and Lopingian. *Acta Sedimentologica Sinica* **32**, 429–41 (in Chinese with English abstract).

Qiu Z, Wang Q, Zou C, Yan D and Wei H (2014b) Transgressive-regressive sequences on the slope of an isolated carbonate platform (Middle–Late Permian, Laibin, South China). *Facies* **60**, 327–45.

Retallack GJ (1994) A pedotype approach to latest Cretaceous and earliest Tertiary paleosols in eastern Montana. *Geological Society of America Bulletin* **106**, 1377–97.

Retallack GJ (2001) *Soils of the Past: An Introduction to Paleopedology, 2nd Edition*, pp. 37–55. Oxford, UK: Blackwell Science Ltd.

Retallack GJ (2008) Cool-climate or warm-spike lateritic bauxites at high latitudes? *The Journal of Geology* **116**, 558–70.

Ritsema CJ and Groenenberg JE (1993) Pyrite oxidation, carbonate weathering, and gypsum formation in a drained potential acid sulfate soil. *Soil Science Society of America Journal* **57**, 968–76.

Robins CR, Deurlington A, Buck BJ and Brock-Hon AL (2015) Micromorphology and formation of pedogenic ooids in calcic soils and petrocalcic horizons. *Geoderma* **251–252**, 10–23.

Ross DJ (2002) *Acid Sulfate Soils, Tannum Sands to St Lawrence, Central Queensland Coast*. Rockhampton, Queensland: Department of Natural Resources and Mines, QNRM02008.

Ross CA and Ross JRP (1995) Permian sequence stratigraphy. In *The Permian of Northern Pangea, Vol. 1* (eds PA Scholle, TM Peryt and DS Ulmer-Scholle), pp. 98–123. Berlin: Springer-Verlag.

Ruxton BP (1968) Measures of the degree of chemical weathering of rocks. *Journal of Geology* **76**, 518–27.

Rygel MC, Fielding CR, Frank TD and Birgenheier LP (2008) The magnitude of Late Paleozoic glacioeustatic fluctuations: a synthesis. *Journal of Sedimentary Research* **78**, 500–11.

Saitoh M, Isozaki Y, Yao J, Ji Z, Ueno Y and Yoshida N (2013) The appearance of an oxygen-depleted condition on the Capitanian disphotic slope/basin in South China: Middle–Upper Permian stratigraphy at Chaotian in northern Sichuan. *Global and Planetary Change* **105**, 180–92.

Saitoh M, Ueno Y, Isozaki Y, Nishizawa M, Shozugawa K, Kawamura T, Yao J, Ji Z, Takai K, Yoshida N and Matsuo M (2014) Isotopic evidence for water-column denitrification and sulfate reduction at the end-Guadalupian (Middle Permian). *Global and Planetary Change* **123**, 110–20.

Sames B, Wagreich M, Wendler JE, Haq BU, Conrad CP, Melinte-Dobrinescu MC, Hu X, Wendler I, Wolfgring E, Yilmaz IÖ and Zorina SO (2016) Review: short-term sea-level changes in a greenhouse world–a view from the Cretaceous. *Palaeogeography, Palaeoclimatology, Palaeoecology* **441**, 393–411.

Sandoval J, O'Dogherty L and Guex J (2001) Evolutionary rates of Jurassic ammonites in relation to sea-level fluctuations. *Palaios* **16**, 311–35.

Shamshuddin J, Muhrizal S, Fauziah I and Van Ranst E (2004) A laboratory study of pyrite oxidation in acid sulfate soils. *Communications in Soil Science and Plant Analysis* **35**, 117–29.

Shao LY, Zhang PF, Ren DY and Lei JJ (1998) Late Permian coal-bearing carbonate successions in southern China: coal accumulation on carbonate platforms. *International Journal of Coal Geology* **37**, 235–56.

Shaw J and Ceman J (1999) Salt-marsh aggradation in response to late-Holocene sea-level rise at Amherst Point, Nova Scotia, Canada. *Holocene* **9**, 439–51.

Sheldon ND (2005) Do red beds indicate paleoclimatic conditions? A Permian case study. *Palaeogeography, Palaeoclimatology, Palaeoecology* **228**, 305–19.

Sheldon ND and Tabor NJ (2009) Quantitative paleoenvironmental and paleoclimatic reconstruction using paleosols. *Earth-Science Reviews* **95**, 1–52.

Shellnutt JG, Denyszyn SW and Mundil R (2012) Precise age determination of mafic and felsic intrusive rocks from the Permian Emeishan Large Igneous Province (SW China). *Gondwana Research* **22**, 118–26.

Shen JW and Xu HL (2005) Microbial carbonates as contributors to Upper Permian (Guadalupian–Lopingian) biostromes and reefs in carbonate platform margin setting, Ziyun County, South China. *Palaeogeography, Palaeoclimatology, Palaeoecology* **218**, 217–38.

Shotyk W (1992) Organic soils. In *Weathering, Soils and Paleosols* (eds IP Martini and W Chesworth), pp. 203–24. Amsterdam: Elsevier.

Siddall M, Rohling EJ, Almogi-Labin A, Hembleben CH, Meischner D, Schmelzer I and Smeed DA (2003) Sea-level fluctuations during the last glacial cycle. *Nature* **423**, 853–8.

https://doi.org/10.1017/S0016756819001481 Published online by Cambridge University Press

Singer M and Janitzky P (1987) *Field and Laboratory Procedures Used in Soil Chronosequence Study*. US Geological Survey Bulletin 1648. Washington, DC: US Government Printing Office, 49 pp.

Sohlenius G and Öborn I (2004) Geochemistry and partitioning of trace metals in acid sulphate soils in Sweden and Finland before and after sulphide oxidation. *Geoderma* **122**, 167–75.

Stoops G, Marcelino V and Mees F (2010) *Interpretation of Micromorphological Features of Soils and Regoliths*. Amsterdam: Elsevier, 752 pp.

Stüben D, Kramar U, Berner Z, Stinnesbeck W, Keller G and Adatte T (2002) Trace elements, stable isotopes, and clay mineralogy of the Elles II K–T boundary section in Tunisia: indications for sea level fluctuations and primary productivity. *Palaeogeography, Palaeoclimatology, Palaeoecology* **178**, 321–45.

Sun YD, Lai XL, Wignall PB, Widdowson M, Ali JR, Jiang HS, Wang W, Yan CB, Bond DPG and Védrine S (2010) Dating the onset and nature of the Middle Permian Emeishan Large Igneous Province eruptions in SW China using conodont biostratigraphy and its bearing on mantle plume uplift models. *Lithos* **119**, 20–33.

Tabor NJ and Montañez IP (2004) Morphology and distribution of fossil soils in the Permo-Pennsylvanian Witchita and Bowie Groups, north-central Texas, USA: implications for western equatorial Pangean palaeoclimate during icehouse–greenhouse transition. *Sedimentology* **51**, 851–84.

Tabor NJ and Montañez IP (2005) Oxygen and hydrogen isotope compositions of Permian pedogenic phyllosilicates: development of modern surface domain arrays and implications for paleotemperature reconstructions. *Palaeogeography, Palaeoclimatology, Palaeoecology* **223**, 127–46.

Tabor NJ, Montañez IP, Scotese CR, Poulsen CJ and Mack GH (2008) Paleosol archives of environmental and climatic history in paleotropical Western Euramerica during the latest Pennsylvanian through Early Permian. *Geological Society of America, Special Paper* **441**, 291–304.

Tabor NJ and Myers TS (2015) Paleosols as indicators of paleoenvironment and paleoclimate. *Annual Review of Earth and Planetary Sciences* **43**, 333–61.

Tabor NJ, Smith RMH, Steyer JS, Sidor CA and Poulsen CJ (2011) The Permian Moradi Formation of northern Niger: paleosol morphology, petrography and mineralogy. *Palaeogeography, Palaeoclimatology, Palaeoecology* **299**, 200–13.

Tan XC, Li L, Liu H, Luo B, Zhou Y, Wu JJ and Ding X (2011) General depositional features of the carbonate platform gas reservoir of the Lower Triassic Jialingjiang Formation in the Sichuan Basin of southwest China: Moxi gas field of the central basin. *Carbonates Evaporites* **26**, 339–50.

Tong JN, Yin HF and Zhang KX (1999) Permian and Triassic sequence stratigraphy and sea level changes of eastern Yangtze platform. *Journal of China University of Geosciences* **10**, 161–9.

Tsatskin A, Sandler A and Avnaim-Katav S (2015) Quaternary subsurface paleosols in Haifa Bay, Israel: a new perspective on stratigraphic correlations in coastal settings. *Palaeogeography, Palaeoclimatology, Palaeoecology* **426**, 285–96.

van Breemen NV (1982) Genesis, morphology, and classification of acid sulfate soils in coastal plains. In *Acid Sulfate Weathering* (eds JA Kittrick, DS Fanning and LR Hossner), pp. 95–108. SSSA Special Publication 10. Madison: Soil Science Society of America.

Walker PH (1972) Seasonal and stratigraphic controls in coastal floodplain soils. *Australian Journal of Soil Research* **10**, 127–42.

Wanas HA and Abu El-Hassan MM (2006) Paleosols of the Upper Cretaceous–Lower Tertiary Maghra El-Bahari Formation in the northeastern portion of the Eastern Desert, Egypt: their recognition and geological significance. *Sedimentary Geology* **183**, 243–59.

Wang Z, Cui Y, Shao L, Zhang D, Dong X and Liu X (2015) Carbonate platform development and sea-level variations of Xisha Islands: based on BIT index of well Xike-1. *Earth Science (Journal of China University of Geosciences)* **40**, 900–8 (in Chinese with English abstract).

Wang Y and Jin Y (2000) Permian palaeogeographic evolution of the Jiangnan Basin, South China. *Palaeogeography, Palaeoclimatology, Palaeoecology* **160**, 35–44.

Wang XD and Sugiyama T (2000) Diversity and extinction patterns of Permian coral faunas of China. *Lethaia* **33**, 285–94.

Wang FD, Zhu XQ and Wang ZG (2011) Madouzi-type (nodular) sedimentary copper deposit associated with the Emeishan basalt. *Science China: Earth Sciences* **54**, 1880–91.

Wang GL, Zhu XQ and Ye F (2009) Interface ore deposits and Emeishan basalt. *Mineral Resources and Geology* **23**, 204–9 (in Chinese with English abstract).

Wardlaw BR, Davydov V and Gradstein FM (2004) The Permian Period In *A Geologic Time Scale 2004* (eds Gradstein F, Ogg J and Smith A), pp. 249–70. Cambridge: Cambridge University Press.

Wendler I, Wendler JE and Clarke LJ (2016) Sea-level reconstruction for Turonian sediments from Tanzania based on integration of sedimentology, microfacies, geochemistry and micropaleontology. *Palaeogeography, Palaeoclimatology, Palaeoecology* **441**, 528–64.

Wignall PB, Védrine S, Bond DPG, Wang W, Lai XL, Ali JR and Jiang HS (2009) Facies analysis and sea-level change at the Guadalupian–Lopingian Global Stratotype (Laibin, South China), and its bearing on the end-Guadalupian mass extinction. *Journal of the Geological Society, London* **166**, 655–66.

Wilson BP, White I and Melville MD (1999) Floodplain hydrology, acid discharge and change in water quality associated with a drained acid sulfate soil. *Marine and Freshwater Research* **50**, 149–57.

Wray JL (1977) *Calcareous Algae*. Developments in Palaeontology and Stratigraphy vol. 4. Amsterdam: Elsevier, 185 pp.

Yamamoto K, Iryu Y, Sato T, Chiyonobu S, Sagae K and Abe E (2006) Responses of coral reefs to increased amplitude of sea-level changes at the Mid-Pleistocene climate transition. *Palaeogeography, Palaeoclimatology, Palaeoecology* **241**, 160–75.

Yang X, Liu JR and Shi GJ (2004) Extinction process and patterns of Middle Permian fusulinaceans in southwest China. *Lethaia* **37**, 139–47.

Zhang KJ (1997) North and South China collision along the eastern and southern North China margins. *Tectonophysics* **270**, 145–56.

Zhao WZ, Xu CC, Wang TS, Wang HJ, Wang ZC, Bian CS and Li X (2011) Comparative study of gas accumulations in the Permian Changxing reefs and Triassic Feixianguan oolitic reservoirs between Longgang and Luojiazhai-Puguang in the Sichuan Basin. *Chinese Science Bulletin* **56**, 3310–20.

Zhou MF, Malpas J, Song XY, Robinson PT, Sun M, Kennedy AK and Keays RR (2002) A temporal link between the Emeishan Large Igneous Province (SW China) and the end-Guadalupian mass extinction. *Earth and Planetary Science Letters* **196**, 113–22.

Zhu GY, Wang TS, Xie ZY, Xie BH and Liu KY (2015) Giant gas discovery in the Precambrian deeply buried reservoirs in the Sichuan Basin, China: implications for gas exploration in old cratonic basins. *Precambrian Research* **262**, 45–66.

Zi JW, Fan WM, Wang YJ, Cawood PA, Peng TP, Sun LH and Xu ZQ (2010) U–Pb geochronology and geochemistry of the Dashibao basalts in the Songpan-Ganzi Terrane, SW China, with implications for the age of Emeishan volcanism. *American Journal of Science* **310**, 1054–80.

https://doi.org/10.1017/S0016756819001481 Published online by Cambridge University Press